Superconducting Transformer Design and Construction

I. E. Chew

A thesis submitted in partial fulfilment
of the requirements for the degree of
Master of Engineering
in
Electrical and Electronic Engineering
at the
University of Canterbury,
Christchurch, New Zealand.

March 2010

ABSTRACT

This thesis first outlines the testing undertaken on a partial core superconducting transformer under open circuit, short circuit, full load and endurance test conditions. During the endurance test, a failure occurred after 1 minute and 35 seconds. During the failure, voltage dipping and rapid liquid nitrogen boil off was observed. This prompted a failure investigation which concluded that the lack of cooling in the windings was the most probable cause to the failure.

Full core transformer and superconductor theories are then introduced. A copper winding transformer model, based on a Steinmetz equivalent circuit and a reverse design method, is described. A superconductor loss model which outlines the different types of losses experienced under AC conditions is used to determine the resistance of the windings in the Steinmetz equivalent circuit. This resistance changes with the magnitude of current and the strength of the magnetic field that is present in the gaps between each layer of the windings. An alternative leakage flux model is then presented, where the flux is modelled based on the combination of the reluctance of the core and the air surrounding the windings. Based on these theories, an iterative algorithm to calculate the resistance of the superconductor is developed.

A new design of a 15kVA single phase full core superconducting transformer, operating in liquid nitrogen, is presented. The issues with building the superconducting transformer are outlined. First, a copper mockup of the superconducting transformer was designed where the mockup would have the same tape and winding dimensions as the superconducting transformer, which means the same core can be used for two different sets of windings. This led to designing a core that could be easily taken apart as well as reassembled. Construction of the core, the copper windings and the superconductor windings ensued. The process of cutting the core laminations, insulating the copper and superconductor tapes, and making the steel fasteners and terminations are described.

The copper mockup and superconducting transformers was then tested under open circuit, short circuit, different load and endurance conditions at both liquid nitrogen and room temperatures. These test results were then compared with the those from two models. The comparison showed a significant inaccuracy in the reactances in the models. This introduced a correction factor into the superconductor model which

made it more accurate. However, further work is required to explain and quantify the correction factors for the copper transformer model under different load conditions.

ACKNOWLEDGEMENTS

I would like to thank everyone who has helped with this project. First I would like to thank my supervisor Professor Pat Bodger and co-supervisor Dr. Wade Enright who have been instrumental in providing support, engineering expertise and proof reading this thesis. Also, none of this would happen without the technical help from the staff at the Electrical and Computer Engineering department, especially Dave Healy, who personally supervised and helped the construction phase of this project. Also, I would like to thank Ken Smart and Jac Woudberg for all the help and constant loaning of equipment. I've also borrowed lots of computer equipment from Peter Kirkstra, thanks to him for putting up with me.

Special thanks go to Andrew Lapthorn, Rowan Sinton, Ryan Van Herel and Lance Frater for helping out with the testing and keeping me out of trouble. I recall, on more than one occasion, where one of them would stop me from blowing stuff up in the machine's lab.

Finally, I'd like to thank Industrial Research Ltd (IRL) and EPECentre for the financial support through the scholarships and funding I received. IRL has also provided me with the copper mockup tape that was used in this project. Without them this project would have been unsuccessful.

CONTENTS

LIST OF FIGURES

LIST OF TABLES

GLOSSARY

The general notation, frequently used terms and abbreviations used in this thesis are listed in this section.

GENERAL NOTATION

V_Z, E_Z	-	Voltage of Z
e_Z	-	Internal voltage of Z
I_Z	-	Current of Z
R_Z	-	Resistance of Z
X_Z	-	Leakage reactance of Z
P_Z	-	Real power of Z
S_Z	-	Apparent power of Z
Q_Z	-	Reactive power of Z
$I_{c,Z}$	-	Critical DC current of Z
B_Z	-	Magnetic field intensity of Z
T_Z	-	Temperature of Z
δ_Z	-	Skin depth of Z
ρ_Z	-	Resistivity of Z
N_Z	-	Number of turns in Z
μ_Z	-	Permeability of Z
l_Z	-	Length of Z
w_Z	-	Width of Z
A_Z	-	Area of Z
ϕ_Z	-	Flux of Z
f_Z	-	Frequency of Z

SYMBOLS

Θ	-	Magnetic field angle with respect to the tape plane
α	-	Function for calculating the DC critical current
ω	-	Angular frequency ($=2\pi f$)
c_{lam}	-	Lamination thickness
n	-	Number of laminations
k_h	-	Material constant for calculating hysteresis loss
x	-	Steinmetz factor
d	-	Superconductor tape thickness

ABBREVIATIONS

BSCCO	-	Bismuth Strontium Calcium Copper Oxide
YBCO	-	Yttrium Barium Copper Oxide
HTS	-	High temperature superconductor
CTM	-	Copper transformer model
SCTM	-	Superconductor transformer model
CTX	-	Copper mockup transformer
SCTX	-	Superconducting transformer
FEA	-	Finite element analysis
ESR	-	Equivalent series resistance
ESL	-	Equivalent series reactance

Chapter 1

INTRODUCTION

Superconductivity was first discovered in 1911 by the Dutch physicist Heike Kamerlingh Onnes. Ever since then, technology utilizing superconductors has kept improving and is being applied in various electrical machines. The biggest known superconducting device, as of 2009, is the Atlas Barrel Toroid, which is a vital superconducting magnet for accelerating particles in the infamous Large Hadron Collider [1].

Accompanying these superconductor applications, there are various theories that describe the superconductivity phenomenon. These theories can be split into different categories for different types of superconductors. Currently, there are type-I and type-II superconductors, which are loosely defined by their respective state transition temperatures. There are two main theories that describe type-I superconductors (BCS [2] and Ginzburg-Landau [3]). There is currently no widely accepted theories for type-II superconductors.

For the application of superconducting transformers, the AC loss theories have been mathematically and empirically modelled. The AC loss theories describe the different losses that the superconductor experiences when the tape is subjected to different currents and external magnetic field strengths. An experimental study on this theory with the Siemens 1MVA superconducting transformer, by Dr. Nanke Oomen [4], is the base work for the superconductor AC loss model covered in this thesis.

1.1 THESIS OBJECTIVE

The objective of the research reported in this thesis is to build two transformers with two windings with the same dimensions, but with different material types, one copper and the other superconductor. The two transformers could then be compared with each other to observe the differences in performance. For ease of construction, one core was built. The idea is that the two different windings wwould have the same dimensions and fit the same core. That way, only the losses of the windings directly affects the performance comparison.

First, a copper mockup transformer was modelled using the reverse design method

and the Steinmetz equivalent circuit. Then the superconductor AC loss theory is used to model the winding resistances of the Steinmetz equivalent circuit. The winding reactance, core reactance and core resistance model is the same for both transformers.

The transformers were rated at 15kVA, operating in liquid nitrogen. The transformer were designed to operate as a 230V/230V isolating transformer. The design of the transformers is presented graphically and the equivalent Steinmetz components are calculated. The performance of the two transformers are then tested in liquid nitrogen and at room temperature. These test results are then compared with the model to gauge how accurate the models are.

1.2 THESIS OUTLINE

Chapter 2 describes the initial work done for an existing partial core superconducting transformer. The partial core superconducting transformer was tested under open circuit, short circuit and full load conditions, and a full load endurance run. The latter resulted in a failure which occurred 1 minute and 35 seconds into the full load endurance run. This prompted an investigation into the transformer failure.

In chapter 3, transformer design theory is presented. The two transformer models are based on the Steinmetz equivalent circuit. The copper mockup transformer was designed following the reverse design method, whereas the superconducting transformer design followed both the reverse design method and superconductor AC loss theory. The superconductor AC losses were converted to winding resistances in the Steinmetz equivalent circuit.

Chapter 4 describes the design and process of the construction of the core, copper windings, and the superconductor windings. The process of cutting the laminations, spacers, insulating the copper and superconductor tape, terminating the winding ends and building of the mechanical supports are described.

Chapter 5 presents the results of the transformer tests. The copper mockup transformer was tested under open circuit, short circuit and full load conditions at both liquid nitrogen and room temperatures. The superconducting transformer was tested under open circuit, short circuit and various load tests at both liquid nitrogen and room temperatures. These results were compared with the model. Anomalies in the comparisons were observed.

Chapter 6 is the general conclusion for the thesis.

Chapter 2

PARTIAL CORE SUPERCONDUCTING TRANSFORMER FAILURE: TESTING AND INVESTIGATION

2.1 INTRODUCTION

An existing 15kVA Bismuth-Strontium-Calcium-Copper-Oxide (BSCCO) superconductor partial core transformer [5] was retested to confirm mathematical models for the core and superconductor. The transformer was operated under no-load, short-circuit and full load conditions, and then subjected to a full load endurance run.

The first no-load, short-circuit and full load tests were only partially successful because of the resolution of the meters were not satisfactory enough to confirm the mathematical models. The transformer failed the endurance run; voltage dipping and rapid liquid nitrogen boil-off was observed one and a half minutes into the test.

An investigative approach was taken to determine the cause of the failure. The radial field at the ends of the partial core was determined not to have caused the tape to go out of its superconducting state. An open circuit test was performed on one of the outside windings which led to the discovery of a shorted turn. The windings and insulation of the transformer were taken apart to visually observe the faulty turns.

2.2 TRANSFORMER DESCRIPTION

Figure 2.1(a) and Table 2.1 show the transformer and its specifications. The superconducting transformer consisted of three windings. The inside winding was rated for 230V and both the middle and outside windings rated for 115V. The middle and outside windings were connected in series, in effect making it a 230V/230V isolating transformer (Figure 2.2). The rated current of the transformer was 65A on all the windings.

The windings of the transformer were made out of BSCCO superconducting tape. This is a Bismuth based, multi-filamentary, high temperature superconductor ceramic encased in a silver alloy matrix. There were four layers in the primary winding and two

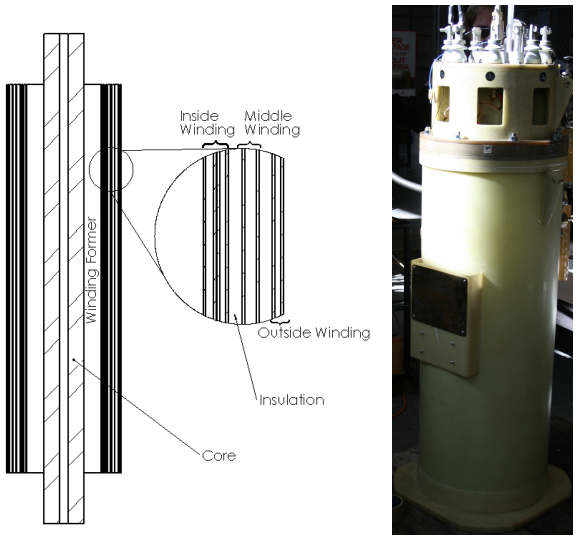

(a) (b)

Figure 2.1 The partial core superconducting transformer.

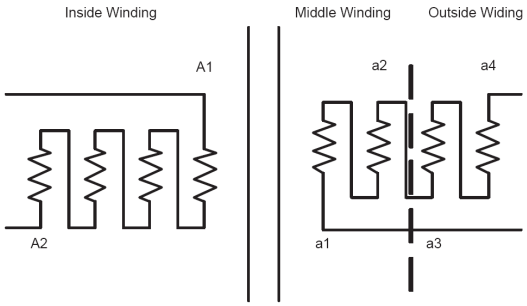

Figure 2.2 Winding configuration; Primary Winding:A1-A2, Secondary Winding: a1-a4

layers for each secondary winding. The windings were insulated with Nomex tape as well as there being Nomex paper between the layers. The layer insulation had varying thicknesses. This is due to having the ends and the layers at the same axial position as the aluminium transformer mockup [6].

The transformer core was made out of 0.23mm thick cold-rolled grain oriented steel laminations. There is only a central core; there are no limbs or yokes. The design of this partial core was to minimise weight as well as core losses. There are 434 laminations and the core length is longer than the winding height of the transformer. This is to reduce perpendicular flux on the ends of the windings. The perpendicular flux decreases the critical current of the tape and must be reduced as much as possible. The core inner radius, shown in table 2.1, is due to a threaded rod that goes right through the middle of the core. The threaded rod is used to lower or lift the core from its dewar.

The partial core transformer was operated at liquid nitrogen temperature, with the transformer windings immersed in the liquid nitrogen inside a cryostat (Figure 2.1(b)).

The core is isolated from the windings and liquid nitrogen by a vacuum chamber which is made out of fibreglass. The temperature of the core cannot be assumed to be at room temperature all the time, in reality the liquid nitrogen will still lower the core temperature below that through heat conduction regardless of the vacuum chamber. A heat model is required to calculate the temperature the core will achieve under different load conditions. The temperature shown in table 2.1 comes from a measured temperature.

There is another vacuum chamber separating the outside atmosphere and the windings which were immersed in liquid nitrogen. The vacuum chambers are designed to insulate the liquid nitrogen as well as isolating the partial core and operating it at room temperature. The two vacuum chambers also contain insulating tissue to minimise heat transfer via convection and reflective mylar which minimises heat transfer via radiation from the outside to the inside.

Table 2.1 Transformer Specifications

Core Specifications		
Lamination Thickness	0.23	mm
Stacking Factor	0.96	
Operating Temperature	-50	°C
Core Length	484	mm
Core Outer Radius	40	mm
Core Inner Radius	8.2	mm

Winding Specifications		
Radial Width	0.3	mm
Axial Height	4.65	mm
Operating Temperature	-196	°C
Length	384	mm
Layer Insulation Thickness	0.2 - 3.45	mm
Number of Layers:		
- Inside Winding	4	
- Middle Winding	2	
- Outside Winding	2	
Total number of layers	8	
Conductor Material	Bi-Sr-Ca-Cu-O	

2.3 TESTING

The open-circuit, short-circuit, full-load and a full-load endurance run were performed on the transformer with the primary voltage applied on the inside winding. The first three tests were partially successful; the results of these tests are shown in Table 2.2.

The open-circuit test (Table 2.2a) shows a primary to secondary voltage ratio of 1.02 indicating near perfect coupling of the flux to both primary and secondary windings. The short-circuit test (Table 2.2b) gives a primary to secondary current ratio of 1.02. The open circuit test voltage ratio indicates that the transformer is a slight step down, hence it is expected that the secondary current should be higher than the primary current. However, this is not the case. Due to the transformer having a partial core, some of the primary current is being diverted for magnetisation (even at such a low excitation voltage). Hence the current ratio is greater than unity. The loaded test (Table 2.2c) indicates an efficiency of 100% and a voltage regulation of 3.2%. However, the losses of the transformer are less than the resolution of the instrumentation used to measure the power. The inaccuracy is mainly due to the transducer used to measure the current. The difference between the primary and secondary real power can be seen in the time series data downloaded from the meter (Figure 2.3).

The conclusion that can be drawn from this is that the sum of the core and winding losses was less than 270W. The open-circuit and short circuit tests showed consistent results with those from the model but the same resolution problem as for the full load test existed. The low value of regulation means that these types of transformer may not need taps to operate within specification, from no-load to full load. However if the supply voltage is not regulated, then tap changers would be required to regulate the output voltage within the specified limits.

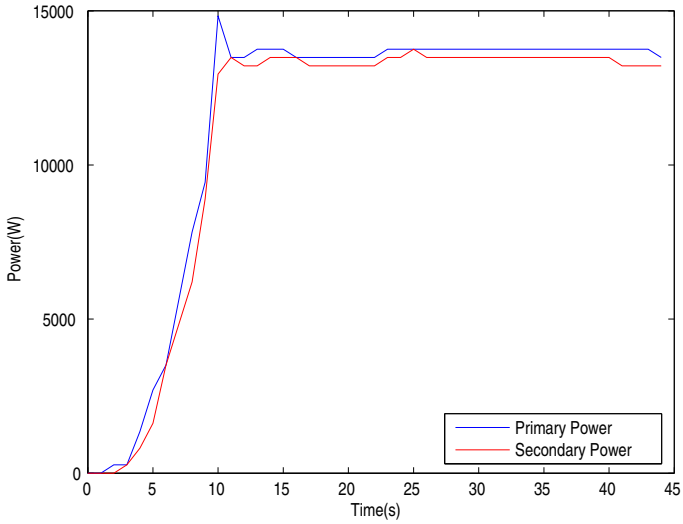

Figure 2.3 Primary and secondary winding full load test power readings from the Fluke 434.

2.3.1 Transformer Failure

The full-load endurance run was commenced with the transformer at rated voltage and load. The failure occurred after 1 minute and 35 seconds. It was observed that the

Table 2.2 Test results for the superconducting transformer.

Open Circuit Test		
Primary Voltage	231	V
Secondary Voltage	226	V
Primary Current	20	A
Primary Real Power	0.2	kW
Primary Apparent Power	4.7	kVA
Primary Power Factor	0.04	

(a)

Short Circuit Test		
Primary Voltage	25	V
Primary Current	66	A
Secondary Current	65	A
Primary Real Power	0.1	kW
Primary Apparent Power	1.7	kVA
Primary Power Factor	0.06	

(b)

Loaded Test		
Primary Voltage	231	V
Primary Current	65	A
Primary Real Power	13.8	kW
Primary Apparent Power	15.1	kVA
Primary Power Factor	0.92	
Secondary Voltage	224	V
Secondary Current	61	A
Secondary Real Power	13.8	kW
Secondary Apparent Power	13.8	kVA
Secondary Power Factor	1.00	
Efficiency	100	%
Regulation	3.2	%

(c)

outside winding voltage decreased at a very fast rate and there was rapid liquid nitrogen boil off. This caused a rapid increase in pressure and popped one of the vents on top of the transformer. The circuit breaker was quickly opened to remove the applied voltage. All the safety valves were opened to relieve the pressure and it was observed that a lot of nitrogen gas escaped. The inside winding was found to be open circuited, which indicated that the whole/part of the winding had been damaged.

2.4 FAILURE INVESTIGATION

There are several reasons for the winding to fail during the full-load endurance run. The winding could have gone out of its superconducting state due to not having enough cooling and exceeding the critical temperature. The radial flux, caused by having a partial core, could have lowered the critical current below the full load current that was flowing in the winding. The radial flux could also cause eddy currents in the silver lattice and stainless steel which might have heated the superconductor and cause it to quench. A manufacturing or process defect could have appeared in the silver lattice or the BSCCO ceramic, giving a section that was more resistive than the good superconductor, and hence the faulty section could melt during testing.

For the radial flux component, there is no physical measurement that could be done as the gaps in between the winding layers are too small for any measuring equipment, and also the inside winding could no longer be energised. There are only simulations and approximations to the magnitude of the radial flux component that could be undertaken. By using Finite Element Modelling and the Magnet[7] program, a flux plot which describes the magnitude and direction was generated (Figure 2.4).

The peak magnitude of the flux as indicated by Magnet was 0.03T at right-angles to the tape plane on the first turn at any end of the inside winding. The critical current is lowered due to this radial flux and is modelled by Oomen et. al.[4]. The formulae described in Oomen et al were obtained via empirical studies on a 1MVA Siemens railway transformer in Germany. The critical current of the superconducting tape is influenced by the direction and magnitude of the applied magnetic field, temperature and the characteristic self-field. The DC critical current is described by Equation 2.1.

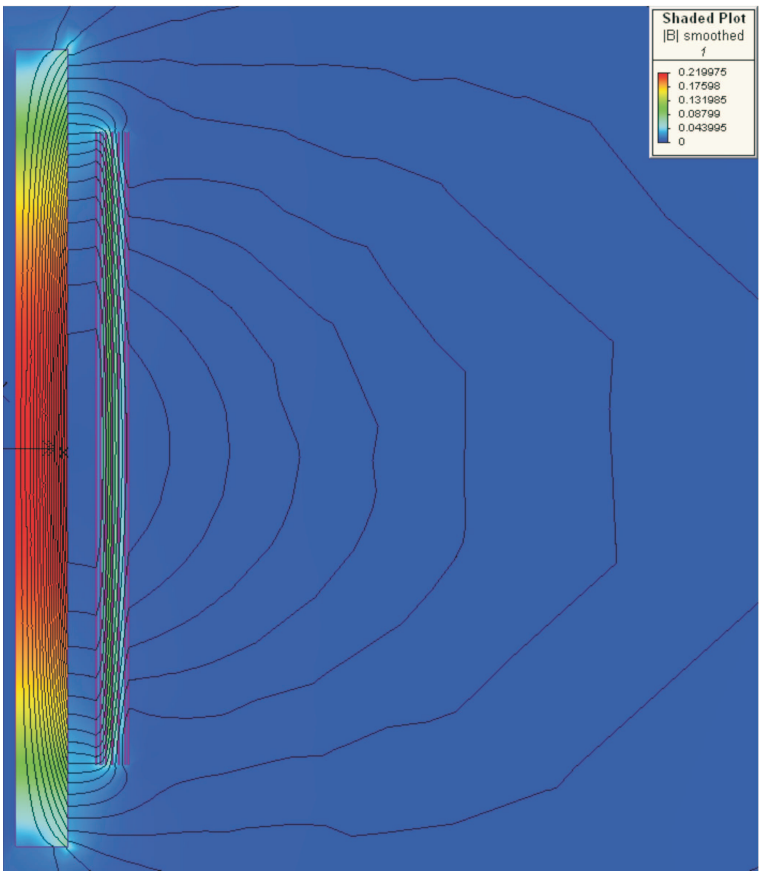

Figure 2.4 Flux plot of the superconducting transformer under full load conditions.

$$I_c(T, B, \Theta) = \frac{I_{c0,77}(3.69 - 0.035T)}{1 + \mid \frac{Bsin(\Theta)}{B_0(T)} \mid^{\alpha(T)}} \tag{2.1}$$

where,

$I_{c0,77}$	=	Rated critical current at self-field, 77K
B	=	Magnetic field strength inside the superconducting tape
Θ	=	Magnetic field angle with respect to the superconducting tape plane
T	=	Temperature of the superconductor

The characteristic magnetic self-field, B_0, is given by the fitted formula[4]:

$$B_0 = 0.03 + (0.0032 - 0.0000393T)I_{c0,77} \tag{2.2}$$

The exponent function in equation 2.1, $\alpha(T)$, is given by[4]:

$$\alpha(T) = 0.2116 + 0.0083T + (0.0012 + 0.00003T)I_{c0,77} \tag{2.3}$$

Using Equation 2.1, the critical current was lowered to 79.03A from its 120A nominal rating. According to the model, the input current waveform would only spend 6 milliseconds per cycle above 79.03A(Figure 2.5). The critical current level shows the time dependance of the AC input current. As the current is a sinusoidal waveform, the critical current level follows the shape of the absolute of the sinusoidal waveform.

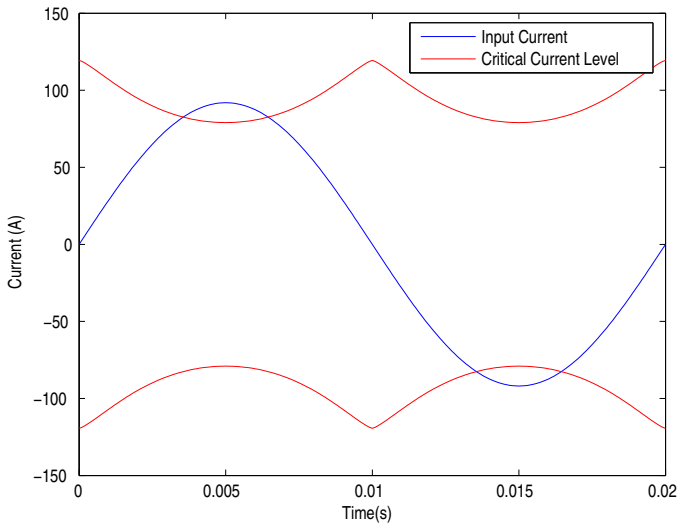

Figure 2.5 The input current waveform of the superconducting transformer exceeding the critical current level calculated in equation 2.1.

Superconductors do not instantaneously go into the quenched state. Heinrich et. al. [8] did several experiments to obtain optical observations on the quench effects of YBCO superconductor. It took 1.1ms for the YBCO to quench and fully generate liquid

nitrogen bubbles (boil-off), 7.7ms after quenching occurs. In Zhou et. al. [9], BSCCO superconductor was forced to quench under short-duration high-current pulses. They also showed that the quenching current drops significantly as the period of the pulses lengthen, and showed that the superconductor has a combined quench and recovery time of less than 1ms. In both papers, the current applied was 1.5 times greater than the rated critical current. The input current applied in the UC transformer winding under consideration was not high enough above the critical current to achieve the same effects as in Heinrich et. al.'s and Zhou et. al.'s experiments.

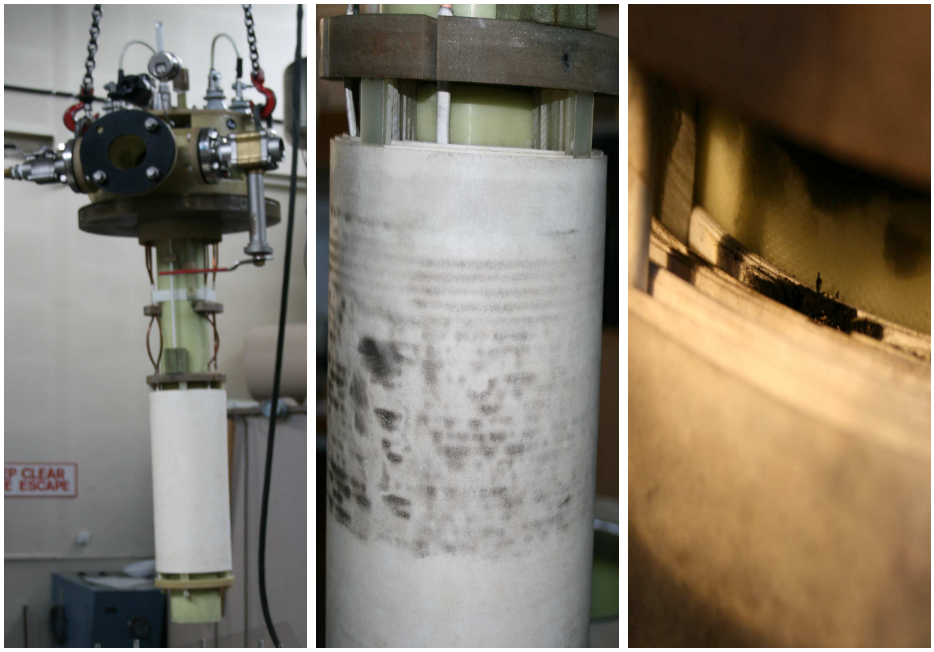

(a) (b) (c)

Figure 2.6 Damage caused to the superconducting transformer during the full-load endurance run;(a) before failure, (b) contaminants sticking onto the insulation after failure and (c) insulation burn damage from the blown superconductor.

The transformer windings were then taken out of the cryostat for investigation (Figure 2.6). Contaminant marks on the insulation are observed in Figure 2.6(b). The carbon scorches and ring marks, due to combustion, gives evidence of the presence of oxygen. With the transformer submerged in liquid nitrogen, some of the oxygen from the atmosphere could have been condensed into liquid form creating a liquid nitrogen and oxygen mix. Another source of oxygen could be from the air voids in the insulation or air bubbles trapped between the insulation and the windings. The air winding chamber was not evacuated, only displaced by the liquid nitrogen when filling. This suggests that the transformer should have had the air evacuated from the chamber prior to filling. Figure 2.6(c) shows burnt out insulation which indicates that a small section of superconductor has burnt which open circuited the winding.

Looking at the construction of the transformer, the windings and insulation were

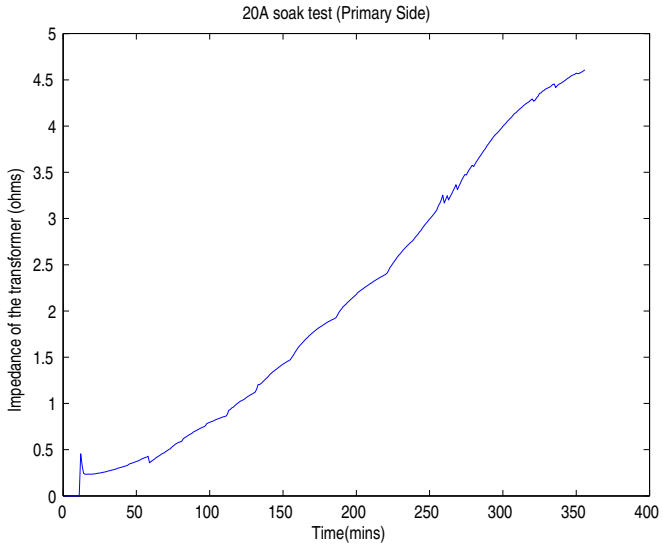

Figure 2.7 Transformer impedance during the 6 hour 20A endurance run

packed tightly together. It did not have any cooling channels for liquid nitrogen in between the windings. Unfortunately there were no temperature readings for the inside windings when the tests were done.

An open circuit test was performed on the outside winding. During this test, it was observed that the current rose dramatically. An applied voltage of 8V resulted in 20A of current drawn in the outside winding. It was also observed that the middle winding was producing 8V which indicated proper voltage transformation. This indicated shorted turns somewhere in the transformer, and given that the inside winding had already been damaged, it was highly possible that the inside winding had shorted turns.

The transformer was then subjected to a 6 hour, 20A endurance run, with an open circuit on the outside winding, in an attempt to measure the temperature at the surface and both ends of the windings. The temperature readings showed that the transformer was fully submerged in liquid nitrogen throughout the entire endurance run. The open circuit current reading showed a decaying transient over time, the voltage had to be stepped up to maintain the current near 20A.

The resulting impedance from these readings shows that it steadily increased over time (Figure 2.7). At the end of the 6 hour test, it was visually observed that the liquid nitrogen was boiling off at a faster rate compared to that at the beginning of the test. This indicated that the shorted turn was no longer superconducting and the silver metal matrix was slowly heating up, hence increasing the overall transformer impedance.

(a) (b) (c)

Figure 2.8 Transformer winding burns (a)outer layer of the middle winding, (b)outermost layer of the inside winding and (c)innermost layer of the inside winding.

2.5 TRANSFORMER UNWINDING

The transformer windings and insulation were taken apart to visually inspect the faulty turn(s). Two layers of the outermost winding (secondary winding) were found unharmed, only superficial damage appeared on the surface of the Nomex paper insulation. The first signs of winding damage appeared on the outer layer of the middle winding (Figure 2.8(a)). Melted glue residue was found on the insulation which indicates that the windings heated the Nomex tape glue to boiling point. The damage to the transformer got worse as more windings and insulation were removed. The Nomex tape on the superconductor on the outermost layer of the inside winding was completely burnt (Figure 2.8(b)). A whole section of superconductor that has been warped due to expansion and contraction is shown in figure 2.8(c). The ends of the innermost layer of the primary winding were burnt and disconnected. Combustion was evident due to the presence of carbon scorches. Figure 2.9 shows the resultant damage on the winding former. The damage appeared to be superficial. The vacuum chamber was still intact

The damage appeared mostly around the center of the inside and middle windings, which suggests that the windings were packed too tightly together to allow sufficient cooling. The ends of the windings were relatively unscathed due to their being exposed directly to liquid nitrogen.

The radial flux cutting the conductors in the middle of the innermost winding is usually low as compared to that in other parts of the windings. Yet the burn patterns

indicate that this particular section of the windings quenched first. This suggests that the quenching did not occur due to the magnetic field. However, the opposite argument could also be made that this section of the winding could have quenched due to the magnetic field strength and burnt out before other sections of the windings could be damaged as they are more exposed to the liquid nitrogen.

All the observations indicated that the superconductor in the inside of the innermost layer quenched due to the temperature rise. A cascading effect ensued, which led to the superconductor burning and disconnecting the primary layer. Further heating caused insulation damage on the outer layers of the inside and middle windings.

Figure 2.9 Damage on the winding former

2.6 CONCLUSION

The results of the failure investigation have been presented and the likely cause of the failure was determined. The Magnet simulation indicates that the radial flux was insufficient to lower the critical current for the superconductor to quench. Further testing indicated that the inside winding had a shorted turn. The windings and insulation were then removed and a visual inspection commenced. There was substantial damage caused to the middle and inside windings. The burn profile indicated that the superconductor quenched due to lack of cooling. The inside winding went out of superconducting state which then caused the winding to fuse and burn out. The resultant heat caused further damage to the subsequent outer layers as well as the middle winding.

Chapter 3

FULL CORE TRANSFORMER MODELING

3.1 INTRODUCTION

Superconductors are classed into two types: type-I and type-II. Type-I superconductors are defined as conventional superconductors that have a transition temperature(T_c) that is below 30K. There are two major theories that describe type-I superconductors: BCS [2] and the Ginzburg-Landau [3] theorem. BCS theory is a microscopic theory which explains the second-order phase transition at the critical temperature. According to the BCS theory, superconductivity is a microscopic effect which results from a Bose condensation of Cooper Pair [10] electrons. The Ginzburg-Landau theory, on the other hand, involves modeling superconductivity using mathematical methods to explain the macroscopic elements of superconductors. However, for type-II superconductors, there is no widely accepted theory (as of 2008) to explain their properties, although there are many papers on this. Type-II superconductors, also known as High Temperature Superconductors (HTS), are defined as having a critical transition temperature above 30K which had been thought un-achievable by BCS-theory. Most HTS are cuprate-based superconductors, but recently ferrite-based superconductors have been discovered [11] [12]. The most common HTS are Yttrium-Barium-Copper-Oxide (YBCO) and Bismuth-Strontium-Calcium-Copper-Oxide (BSCCO) with critical temperatures at 92K and 110K respectively.

This chapter gives a description of the parameters taken into consideration for building a superconducting transformer. A copper transformer mockup (CTM) design of the HTS transformer is firstly proposed to ensure good insulation, cooling and core design.

3.2 COPPER TRANSFORMER MODEL

The CTM is designed to be a 15kVA, full core, 230V/230V isolating transformer. The windings are submerged in liquid nitrogen and are assumed to be operating at the boiling temperature (77K). The CTM design is based on the Steinmetz equivalent circuit (Figure 3.1) and the reverse design method [13]. Because of the low supply

frequency, the Steinmetz equivalent circuit ignores all capacitive effects that do not have a significant impact.

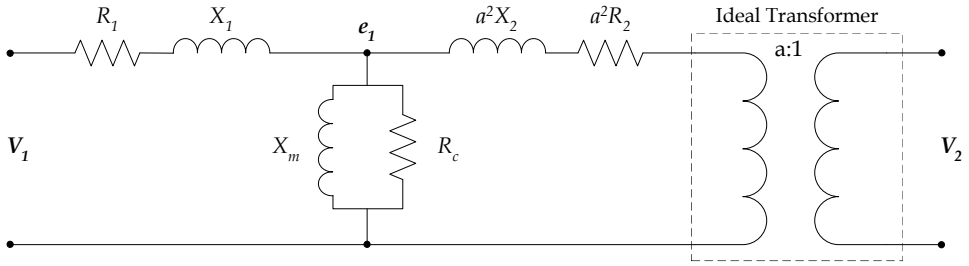

Figure 3.1 The Steinmetz equivalent circuit for a transformer.

3.2.1 Winding Resistances

The resistance of the windings, R_1 and R_2, can be calculated from:

$$R = \rho \frac{l}{A} \quad (\Omega) \tag{3.1}$$

where,

ρ	=	resistivity of the conductor	(Ωm)
l	=	length of the conductor	(m)
A	=	cross sectional area of the conductor	(m^2)

The resistivity of the conductor, ρ, is dependant on temperature and is given by:

$$\rho = \rho_{20^\circ C}(1 + \triangle\rho(T - 20)) \quad (\Omega m) \tag{3.2}$$

where,

$\triangle\rho$	=	thermal resistivity coefficient	($/^\circ$C)
$\rho_{20^\circ C}$	=	material resistivity at 20°C	(Ωm)

However, it was found that equation 3.2 incorrectly models the resistivity of copper at very low temperatures [14] due to the incorrect values used for the thermal resistivity coefficient. Equation 3.2 is then remodeled based on the experimental results in [14], where the copper resistivity is now:

$$\rho = 6.99 \times 10^{-11} T + 1.57 \times 10^{-8} \Omega m \tag{3.3}$$

where,

T = Operating temperature (°C)

The resistivity of the windings can be modelled using Equation 3.2 at room temperature and Equation 3.3 at liquid nitrogen temperature.

3.2.2 Eddy Current and Hysteresis Losses

The resistance, R_c, is a resistance representing the eddy current and hysteresis losses of the core. The component due to eddy currents depends on the skin depth and the thickness of the lamination. The skin depth is given by:

$$\delta_{ec} = \sqrt{\frac{2\rho_c}{\mu_0 \mu_{rc} \omega}} \quad (m) \tag{3.4}$$

where,

ρ_c	=	resistivity of steel or core material	(Ωm)
ω	=	angular frequency, $2\pi f$, where f is the supply frequency	(rad/s)

For skin depth greater than half the lamination thickness, the eddy current resistance is given by [15]:

$$R_{ec} = \frac{12\rho_c {N_1}^2 A_c}{l_c \times {c_{lam}}^2} \quad (\Omega) \tag{3.5}$$

where,

N_1	=	number of primary turns	
A_c	=	cross sectional area of the core	(m^2)
l_c	=	effective flux path length	(m)
c_{lam}	=	lamination thickness	(m)

The skin depth changes with changing frequency or resistivity of the core material. With a set supply frequency, only the resistivity directly affects the skin depth. At very low temperatures, the resistivity becomes small enough to make the skin depth less than half of the lamination thickness. The eddy current path becomes smaller creating a non-uniform flux distribution in the core, as the eddy currents tend to flow near the surface of the laminations. In this case, Equation 3.5, is replaced by [16]:

$$R_{ec} = \frac{2{N_1}^2 \rho_c}{l_c} \left(\frac{n b_{core} + w_{core} - 2n\delta_{ec}}{\delta_{ec}} \right) \quad (\Omega) \tag{3.6}$$

where,

This equation is only valid for square cross-sectional area cores. For circular cores, the fraction of flux penetration into the lamination is used to calculate the effective cross sectional area. Hence the eddy current resistance is:

n	=	number of laminations	
b_{core}	=	breadth of the core	(m)
w_{core}	=	width of the core	(m)

$$R_{ec} = \frac{12\rho_c {N_1}^2 A_c}{l_c \times {c_{lam}}^2} \times \%FluxPenetration \quad (\Omega) \tag{3.7}$$

where,

$$\%FluxPenetration = \frac{\delta_{ec}}{\frac{c_{lam}}{2}} \tag{3.8}$$

This method is not entirely correct and is subject to error. A better way of doing this would be to change b_{core} in equation 3.6, for different steps in a circular core. However, the total core resistance, R_c in figure 3.1, is usually dominated by the hysteresis resistance which is described later. Hence the error in equation 3.8 can be ignored.

In designing the CTM there are two options; to operate the transformer core at room or at liquid nitrogen temperature. A comparison between the two options is needed to maximise efficiency.

If the steel resistivity, ρ_c, was calculated using equation 3.2, it produces an unrealistic negative value at liquid nitrogen temperatures. This is due to the same problem experienced in section 3.2.1. The steel resistivity was corrected to [14]:

$$\rho_{c\_-196^\circ C} = 4.5 \times 10^{-8} \Omega m \tag{3.9}$$

With this correction, all the variables in equation 3.5 and 3.7 are set constant except for the temperature, which is set to 20°C and -196°C respectively. Table 3.1(b) shows the difference in selected parameters due to the two operating temperatures.

The eddy current resistance changes by an order of magnitude when operated in liquid nitrogen and this is mainly due to the effect of temperature on the resistance of the steel. The correction to the resistivity of steel in equation 3.9 might not be correct since the steel used might have a different resistivity to that measured in [14]. The core resistance is usually dominated by the hysteresis resistance and the error introduced by equation 3.9 would be insignificant.

Core Dimensions		
Core Diameter	75	mm
Stacking Factor	0.85	
Number of Primary Turns, $N1$	296	
Lamination Thickness, c_{lam}	0.23	mm
Number of Laminations, n	277	
Total Core Length, l_c	783.78	mm
Core Cross Sectional Area, A_c,	4418	mm^2

(a)

Operating Temperature	Room (20°C)	Liquid Nitrogen (-196°C)	
Core Resistivity, ρ_c	4.8×10^{-7}	4.5×10^{-8}	Ωm
Penetration Depth, δ_{ec}	0.4026	0.1068	mm
Eddy Current Resistance, R_{ec}	45700	3980	Ω

(b)

Table 3.1 Core operating temperature comparison: (a) Core dimensions and (b) Eddy current resistance comparison.

The hysteresis losses are modelled as a resistance, R_h, and is given by [16]:

$$R_h = \frac{{e_1}^2}{k_h f {B_c}^x \times WT_c} \quad (\Omega) \tag{3.10}$$

where,

e_1	=	internal primary winding voltage	(V)
k_h	=	material constant (0.02 to 0.11 for steel)	
B_c	=	magnetic field intensity	(T)
x	=	Steinmetz factor (varies between 1.8 and 2.5)	
WT_c	=	weight of the core	(kg)

3.2.3 Core and Winding Reactances

The magnetising reactance, X_m, for a full core transformer [15] is given by:

$$X_m = \frac{\omega {N_1}^2 \mu_0 \mu_{rc} A_c}{l_c} \quad (\Omega) \tag{3.11}$$

where,

μ_0	=	permeability of free space	($4\pi \times 10^{-7}$ H/m)
μ_{rc}	=	relative permeability of core	(H/m)

The leakage reactances, X_1 and X_2, are calculated from a total transformer leakage reactance, X_{12} [13]. The total leakage reactance is (see figure 3.2):

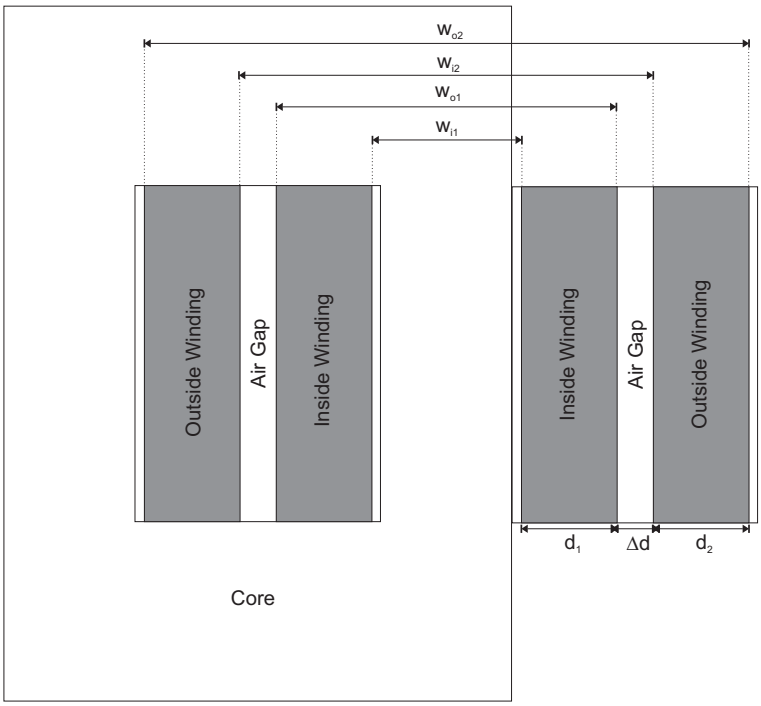

Figure 3.2 Dimensions of a typical core type transformer which are used for calculation of the total transformer leakage reactance, X_{12}

$$X_{12} = \frac{\omega \mu_0 N_1^2}{l_c} \left[\frac{l_p d_1 + l_s d_2}{3} + l_{ps} \Delta d \right] \tag{3.12}$$

where,

l_p	=	mean circumferential length of the inside winding	(m)
l_s	=	mean circumferential length of the outside winding	(m)
l_{ps}	=	mean circumferential length of the interwinding space	(m)

For circular cross section cores:

$$l_p = \pi \left(\frac{w_{i1} + w_{o1}}{2} \right) \tag{3.13}$$

$$l_s = \pi \left(\frac{w_{i2} + w_{o2}}{2} \right) \tag{3.14}$$

$$l_{ps} = \pi \left(\frac{w_{o1} + w_{i2}}{2} \right) \tag{3.15}$$

The leakage reactances of the inside and outside winding are usually assumed to be equal [13]:

$$X_1 = X_2 = \frac{X_{12}}{2} \tag{3.16}$$

3.3 SUPERCONDUCTING TRANSFORMER MODEL

There are several design considerations that need to be taken into account for a superconducting transformer design. The most important factor is cooling, the operating temperature of the HTS tapes must be kept under the critical temperature at all times. This section describes the modeling of the tape, which is only concerned with the tape losses. The thermal issues are covered in later chapters. Most of the superconductor modeling is based on the work carried out by Oomen [4] which is based on a superconducting transformer built by Siemens AG.

3.3.1 DC Properties

The DC properties of the superconducting tape are needed to calculate some of the AC losses. Mainly the critical DC current is used for the AC calculations.

The critical current, critical temperature and magnetic field intensity are the boundary conditions in which the superconducting tape will remain in a superconducting state. However, the critical DC current is actually dependant on the other two boundary conditions mentioned. It is described by the equation:

$$I_c(T, B, \Theta) = I_{c0,77} F(T) G(T, B, \Theta) \quad (A) \tag{3.17}$$

where,

$I_{c0,77}$	=	Critical DC current in self field at 77K
Θ	=	Angle between the magnetic field and the tape plane
T	=	Temperature
B	=	Magnetic field intensity

The functions F(T) and G(T,B,Θ) in equation 3.17 are defined by:

$$F(T) = 5.92 - 0.065T \text{ for T<75K} \tag{3.18}$$

$$F(T) = 3.69 - 0.035T \text{ for T>75K} \tag{3.19}$$

and

$$G(T, B, \Theta) = \frac{1}{1 + |Bsin(\Theta)/B_o(T)|^{\alpha(T)}} \text{ for } \Theta > \Theta_c \tag{3.20}$$

$$G(T, B, \Theta) = \frac{1}{1 + |Bsin(\Theta_c)/B_o(T)|^{\alpha(T)}} \text{ for } \Theta < \Theta_c \tag{3.21}$$

where, B_o is the characteristic magnetic field, which is empirically obtained and given by [4]:

$$B_o(T) = 0.03 + (0.0032 - 0.000393T)I_{c0,77} \tag{3.22}$$

The temperature dependance of G(T,B,Θ) is a function which is also empirically obtained:

$$\alpha(T) = 0.2116 + 0.0083T + (0.0012 + 0.00003T)I_{c0} \tag{3.23}$$

These empirically obtained equations might not suit the modelling here, however, as a base approach it is an acceptable starting point.

3.3.2 AC Losses

There are different types of AC losses associated with superconducting tape. There are many theories available and engineering formulas that have been developed to describe these losses. The one thing that many theories have in common is the dependance of these losses on the direction and amplitude of an alternating magnetic field combined with an alternating current. There are many methods, which are mostly empirical such as the pickup coil method [17] [18], which can determine the total loss density of the tape, but very little on individual loss components. In this section, the effects of self induced and external magnetic fields on different types of BSCCO tape losses are described.

3.3.2.1 Self Field Loss

The self field loss is associated with the magnetic field that is generated by the tape itself when an alternating current is passed through the tape. This is independent of external magnetic fields and is due to the penetration of the magnetic field into the tape [19].

The self field loss is described by [4] and simplified to:

$$P_{sf} = \frac{\mu_0 f}{4\pi} \frac{I_{a,sc}^{3.5}}{I_{c,avg}^{1.5}} l_{sc} \quad (W) \tag{3.24}$$

where,

$I_{a,sc}$	=	current amplitude through the superconducting filaments (A)
$I_{c,avg}$	=	average critical current of the superconductor (A)
l_{sc}	=	total length of the superconductor (m)

$I_{a,sc}$, is assumed to be the total current through the tape, as most of the current if not all are going through the superconducting filaments anyway. Only a very tiny proportion of the current is traveling through the metal matrix of the superconductor. For accuracy, the current through the filaments can be calculated using [4]:

$$10^{-4}\left(\frac{I_{sc}}{I_c(T,B,\Theta)}\right)^{n(T,B,\Theta)} = R_m(I - I_{sc}) \quad (Vm^{-1}) \tag{3.25}$$

where,

I_{sc}	=	current through the superconducting filaments	(A)
R_m	=	Resistance per meter of the silver matrix	(Ωm^{-1})
I	=	The transport current carried by the whole cable	(A)
$n(T,B,\Theta)$	=	n-value, power index of the superconductor	

Equation 3.25 describes the electric fields associated with the superconductor. The left hand side of the equation describes the electric field of the superconductor filaments which is caused by flux creep. The right hand side of the equation is the electric field of the silver matrix. The electric field along the tape, E, is then given by either the right hand side or the left hand side of equation 3.25. Thus current through the superconductor filaments, I_{sc}, can be obtained by solving all the other variables iteratively. This process is time consuming and not really relevant, as mentioned before, because in the superconducting state, all the current will be flowing in the filaments.

3.3.2.2 Resistive Loss

The resistive loss component is present with both AC and DC currents [20]. The resistive loss is calculated using:

$$P_R = EIl_{sc} \text{ for DC} \quad (W) \tag{3.26}$$

and

$$P_R = fl_{sc}\int_{t=0}^{1/f} E(t)I(t)dt \quad \text{for AC} \quad (W) \tag{3.27}$$

where the electric field, E, is calculated using equation 3.25. The resistive loss component is only significant if the transport current is a lot higher than the critical current [4].

3.3.2.3 Dynamic Resistance

The dynamic resistance is the resistance due to the interaction between the current and the external magnetic field [4]. In effect, an increase in magnitude of the magnetic field results in an increase in the losses and hence the overall resistance, R_1 and R_2, in the Steimetz equivalent circuit. The dynamic resistance power loss is modelled based on the critical state model and is usually measured [19]. The dynamic resistance power loss is described as:

$$P_{dyn} = (C_5 cos(\Theta) + C_6 sin(\Theta)) B_a I_a^2 V \quad (W) \tag{3.28}$$

where,

V	=	Total volume of the superconductor tape
C_5,C_6	=	Constants obtained from measurements

Equation 3.28 can be simplified to:

$$P_{dyn} = P_{dyn,\,||} + P_{dyn,\,\perp} \tag{3.29}$$

where P_{dyn} is the sum of both the parallel and perpendicular components of the dynamic resistance power loss. The components of equation 3.29 can be expressed as:

$$P_{dyn,\,||} = A_{fr,\,||} \frac{f_{gw} d l_{sc}}{I_{c,avg}} B_a I_{a,sc}^2 \quad (W) \tag{3.30}$$

and

$$P_{dyn,\,\perp} = A_{fr,\,\perp} \frac{f_{gw} w l_{sc}}{I_{c,avg}} B_a I_{a,sc}^2 \quad (W) \tag{3.31}$$

where,

$A_{fr,\,\|\|}$	=	Fraction of superconductor filaments occupying the thickness of the superconducting tape.	
$A_{fr,\,\perp}$	=	Fraction of superconductor filaments occupying the width of the superconducting tape.	
d	=	Thickness of the superconductor tape	(m).
w	=	Width of the superconductor tape	(m).

The area fraction orientations, $A_{fr,||}$ and $A_{fr,\perp}$, are better explained in figure 3.3. Typical values for $A_{fr,||}$ and $A_{fr,\perp}$, for elliptic section superconductor filament areas, are 0.65 and 0.85 respectively [4].

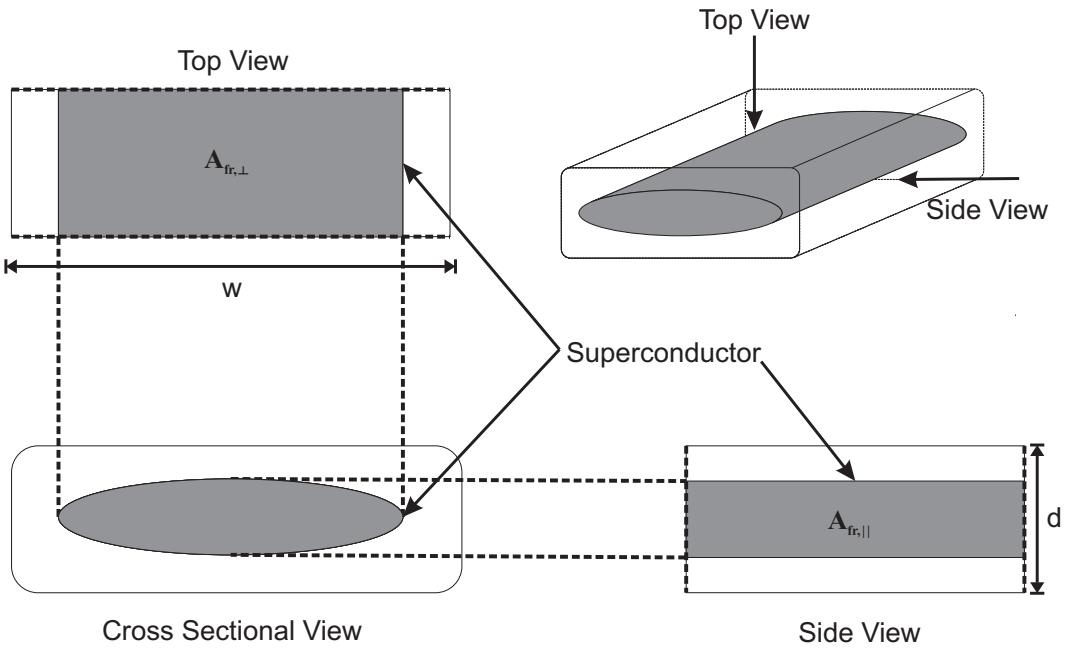

Figure 3.3 Graphic representation of the fraction, $A_{fr,||}$ and $A_{fr,\perp}$, of space occupied by superconducting filaments

3.3.2.4 Eddy-current Loss

The eddy-current loss is due to the currents induced by external magnetic fields in the metal matrix of the superconductor. Here, the induced eddy-currents are assumed to be low frequency (<70Hz) and the skin depth is significant larger than half the thickness of the tape [4]. The calculations and equations are based on estimates from [21]. The equations for both perpendicular and parallel components are:

$$P_{E,\,||} = \frac{\pi^2 f_{gw}^2}{6\rho_m} B_{a,||}^2 d^3 w l_{sc} \quad (W) \tag{3.32}$$

$$P_{E,\,\perp} = \frac{\pi^2 f_{gw}^2}{6\rho_m} B_{a,\perp}^2 w^3 d l_{sc} \quad (W) \tag{3.33}$$

where ρ_m is the resistivity of the metal matrix of the superconductor which is the resistivity of the silver ($\approx 4 \times 10^{-9}$ Ω m at 77K).

3.4 MAGNETIC FIELD MAGNITUDE AND ORIENTATIONS

The field directions and magnitudes are required for certain calculations of the AC losses of superconductors. This section describes the theory and equations to calculate field direction and magnitudes in a full core transformer. Only a core type transformer is being considered here, and it is assumed it is being operated in the linear region of the B-H curve of the core. Figure 3.4 shows the flux paths of a typical core type

transformer. The ideal transformer assumes that the excited winding links all the flux through the windings and the core, however in reality this is not the case. Some of the flux traverses out of the magnetic circuit into free air or open space. This is termed leakage flux which is shown as Φ_1 and Φ_2 for the inside winding and outside winding respectively. In this section, the equations used to calculate the magnitudes of the leakage magnetic field strengths Φ_1 and Φ_2 are described.

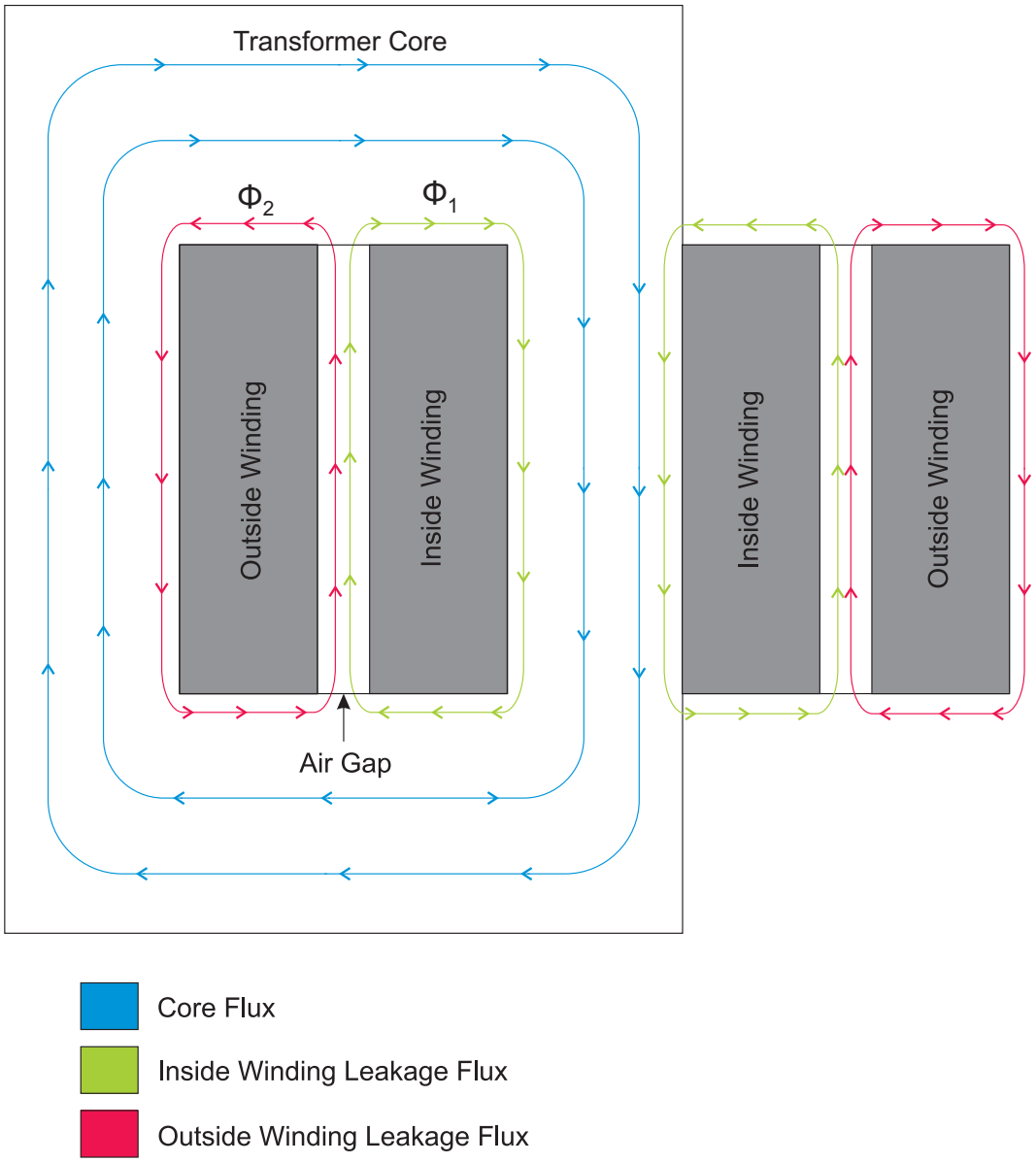

Figure 3.4 Core flux, inside winding leakage flux and outside winding leakage flux paths

3.4.1 Parallel Fields

The parallel field is defined as the magnetic field that is parallel to the tape plane, assuming that rectangular conductors are used. There is very little theory on how to

calculate the field strength (T) inside the windings. Using magnetic circuit theory, an attempt in calculating the field strength is made here. The reluctance through a medium is:

$$\mathfrak{R} = \frac{l}{\mu_r \mu_0 A} \quad (\mathrm{H}^{-1}) \tag{3.34}$$

where,

l	=	length of the flux path	(m)
μ_0	=	permeability of free space ($= 4\pi \times 10^{-7}$)	(H/m)
μ_r	=	relative permeability of the medium (= 1 for air)	
A	=	cross sectional area of the flux	(m^2)

The magnetomotive force (mmf) is equal to:

$$mmf = NI \quad \text{(A-turns)} \tag{3.35}$$

and

$$mmf = \Phi\mathfrak{R} \tag{3.36}$$

The leakage flux density is shown in equation 3.37.

$$B = \frac{\Phi}{A} \quad (T) \tag{3.37}$$

By substituting equations 3.35 and 3.36 into equation 3.37, the flux density is redefined as:

$$B = \frac{NI}{\mathfrak{R}A} \quad (T) \tag{3.38}$$

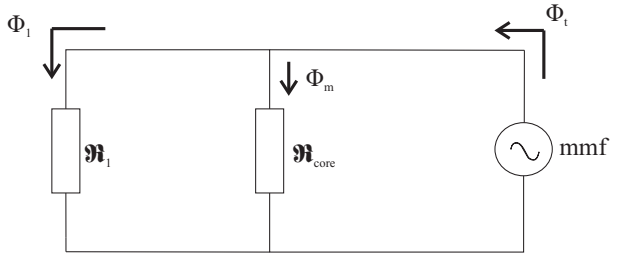

Figure 3.5 Magnetic circuit of a full core transformer taking into account the interwinding gap through which most of the stray flux flows

From figure 3.4, the leakage flux encloses the steel and the air gap. Assuming that the fringing effect of the flux is minimal, the reluctance, $\mathfrak{R}_1$ is a combination of both the reluctance of the steel and the air. For a core type transformer, the leakage flux is not-symmetrical around the core. This is due to the non-symmetrical nature of the core

type transformer. The leakage flux on the inside of the transformer winding window flows through more steel compared to the leakage flux not enclosed by the core.

For the most accurate modelling of the flux, a three dimensional flux path would be simulated. As a base approach to this problem, it is assumed that the leakage flux travels through approximately half of the steel core, meaning that, $\mathfrak{R}_1$ is now equal to:

$$\mathfrak{R}_1 = \frac{\mathfrak{R}_{core}}{2} + \mathfrak{R}_{air} \quad \text{(A-turns/Wb)} \tag{3.39}$$

$\mathfrak{R}_{core}$ is significantly smaller than $\mathfrak{R}_{air}$ (usually in orders of magnitude if the core is made out of steel) hence $\mathfrak{R}_1$ is approximately equal to $\mathfrak{R}_{air}$.

Due to construction, thermal and insulation requirements, transformers might have radial spaces in between layers and windings. This affects the leakage reactance (refer to section 3.2.3) and also the magnetic field distribution [22]. The field distribution increases in steps from the innermost winding shown in figure 3.6, and peaks where the interwinding space meets the end of the energised winding. It is assumed that the peak leakage field strength is that calculated using equation 3.38. Assuming that the inter-layer spaces are the same, the leakage field strength is a fraction of the peak, depending on the number of layers. For example, if the energised winding has 5 winding layers, the end of the first layer would experience 1/5th of the peak value.

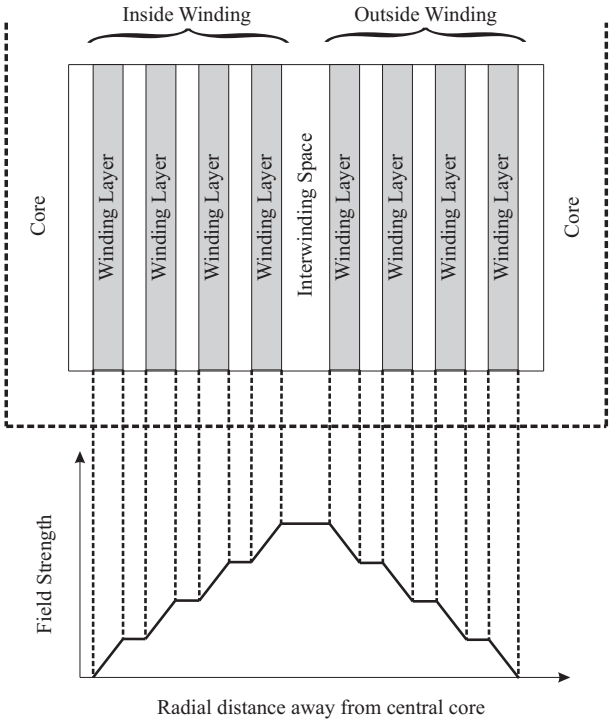

Figure 3.6 Leakage field distribution of a typical core type transformer

3.4.2 Perpendicular Fields

The perpendicular field is defined as the magnetic field that is normal to the tape plane. Here the fringing is ignored, hence the field is assumed to have an angle of 90° with respect to the tape plane. As a worse case scenario, only the ends of the windings are affected by this perpendicular field and the field strength can be assumed to be the same magnitude as the parallel fields. In reality, most of the perpendicular field will be flowing in the steel and not through the winding itself. Hence the critical current would not be de-rated as much in comparison with the model.

3.5 ITERATIVE SUPERCONDUCTOR MODEL

The superconductor model requires a current magnitude to calculate the AC losses, and hence effectively, the resistance of the transformer. However, the resistance and current are dependant on each other. To account for this, an iterative approach is needed to determine the full model.

Initially, both winding resistances, R_1 and R_2, are set to zero. All the other parameters are calculated based on winding and core dimensions. The currents through the windings are then calculated given an applied voltage. The magnetic fields (parallel and perpendicular) are calculated for the superconductor AC losses. The AC losses are translated to values of R_1 and R_2. Then, the winding currents are recalculated. If the differences in the resistance values between the current iteration and the previous iteration do not meet the tolerance required, then the loop continues until the tolerance is met.

3.6 CONCLUSION

The superconductor DC parameters were described. These parameters are necessary to calculate the AC loss components of the superconducting tape. There are no loss components for DC conditions. The AC losses, which include self-field, resistive, dynamic-resistance, hysteresis and eddy current losses, are described.

Most of the AC losses described for BSSCO tape require a field strength value to calculate the losses. A leakage flux model is given to provide the information on these magnetic fields in the spaces in between the windings. The main assumption is that the fringing effects, typically seen in solenoids, are not present.

Finally, a flow chart describing the iterative process of calculating R_1 and R_2 of the superconductor tape under AC conditions was presented.

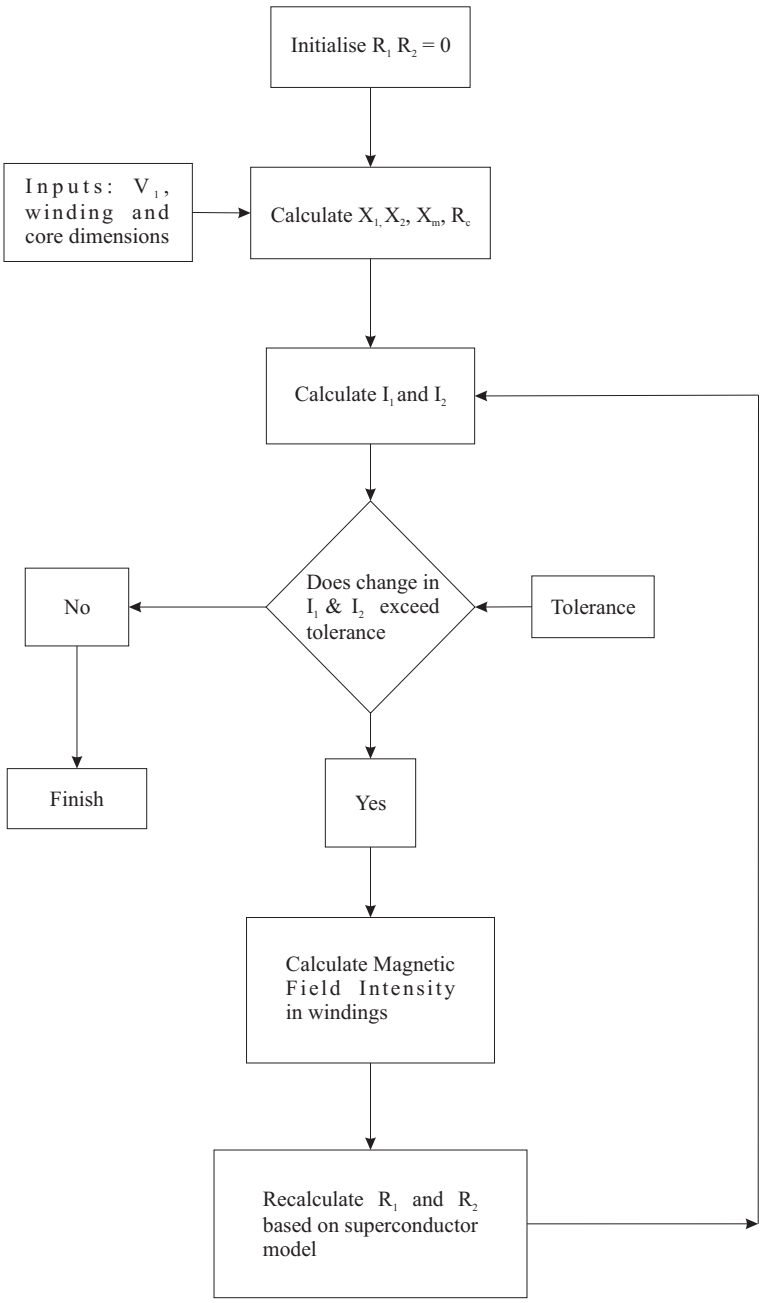

Figure 3.7 Flow chart showing the iterative process for the superconductor model

Chapter 4

FULL CORE SUPERCONDUCTING TRANSFORMER DESIGN AND CONSTRUCTION

4.1 INTRODUCTION

A detailed design of a 15kVA single phase superconducting transformer, using Computer Aided Design (CAD) and mathematical modelling, is described in this chapter. The issues involved with building superconducting transformers are addressed. Details of the design of a copper mockup transformer and the superconducting transformer are given. The idea is to compare two transformers with the same core and winding dimensions, but with different winding material types. A CAD graphic representation is presented, using the program SolidWorks^{TM}. The details of the construction, which includes insulating the wire and cutting the steel laminations, are presented.

4.2 DESIGN ISSUES

Superconductors have specifications such as the minimum bend radius and the critical temperature. The minimum bend radius may pose challenges during the construction period, as the wire would need to be handled with care. The design of the cooling of the transformer needs to keep the windings below or at the specified temperature at all times, regardless of the load. Other issues to be addressed are the wire insulation, and keeping the leakage flux to a minimum so the wire would not quench.

As discussed in chapter 2, it is important not to over-insulate and disrupt the cooling of the superconducting wire. This can cause a quench avalanche [8] destroying the winding. However, depending on the design and purpose of the transformer, the windings do require some interwinding electrical insulation. It is known from previous work that liquid nitrogen has a higher breakdown strength than conventional transformer oil [23]. It was also found that liquid nitrogen has a breakdown strength ~20kV/mm depending on how pure the liquid nitrogen is [24]. Based on this, the design can utilise and maximise the benefits of liquid nitrogen as its coolant.

The next issue is that superconducting tape is made out of a combination of ceramic

and metal materials. This causes the tape to be very brittle. There is a minimum bend radius associated with the tape. Therefore the tape must be handled with care and any process that requires bending the tape must ensure that the specification of the minimum bend radius is met. Other than breaking the superconductor, the bend radius also affects the critical current of the superconductor [25]. The superconductor DC critical current decreases if the tape bent past the minimum bend radius.

4.3 TRANSFORMER DESIGN

The initial approach to the transformer design was to have a container for the windings and the coolant. This would thermally separate the core from the windings. A CAD for the transformer, including the container, was proposed as shown in figure 4.1.

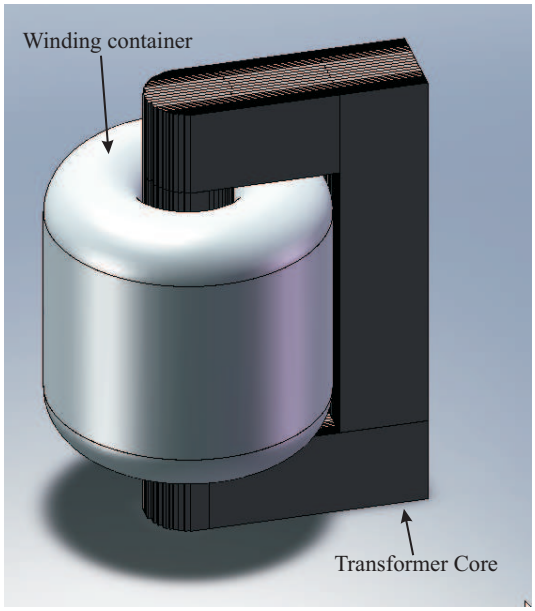

Figure 4.1 Full core transformer, with toroid shape top and bottom winding container

The bottom and top of the container are in the shape of a toroid for distributing the forces of contraction, due to cooling, evenly around the container to prevent the container from cracking. The container was to be made out of fibreglass composite material. It was known from previous work that such a container could withstand the mechanical stresses associated with cryogenic temperatures [5].

Using a container adds another complexity to the design as the thickness of the container walls determines how cold the middle of the core gets as well as how fast the liquid nitrogen boils-off. It also contributes to an increase in the leakage reactance due to having larger winding windows, as compared to having no container. A cost comparison, in terms of capital cost and running costs, would be beneficial in determining a final design. However, the container manufacturing cost was deemed to be too high,

and it was decided that it would not be viable for this project. The next step was to put the whole transformer, including the core, into liquid nitrogen.

It is desirable to minimise the core losses, in effect minimising liquid nitrogen boil-off. The core losses are usually dominated by hysteresis losses. From chapter 3, it is known that the hysteresis loss is dependant on the weight of the core. The heavier the weight of the core, the higher the power loss. However, reducing the weight of the core means reducing the core cross-sectional area. This reduces the reluctance and runs the risk of saturating the core. Hence, the core design must strike a balance between minimal power losses and keeping the core from saturating.

Previous research has been undertaken to record the core losses under liquid nitrogen conditions [26]. The study showed that there was no substantial increase in core losses when operating in liquid nitrogen as compared to operating at ambient room temperature. This is due to the skin depth working in opposition to the resistivity of the steel, i.e. the skin depth decreases (causing the resistance to increase) when the resistivity decreases (due to the low temperature) resulting in a minor change in core loss as compared to room temperature operation.

To keep the windings at liquid nitrogen temperature, layer gaps or cooling channels were made to keep the coolant in direct contact with the windings. The windings, shown in figure 4.2, are separated by composite fibreglass flat bars or "spacers". The cooling channels are vertical and evenly spaced.

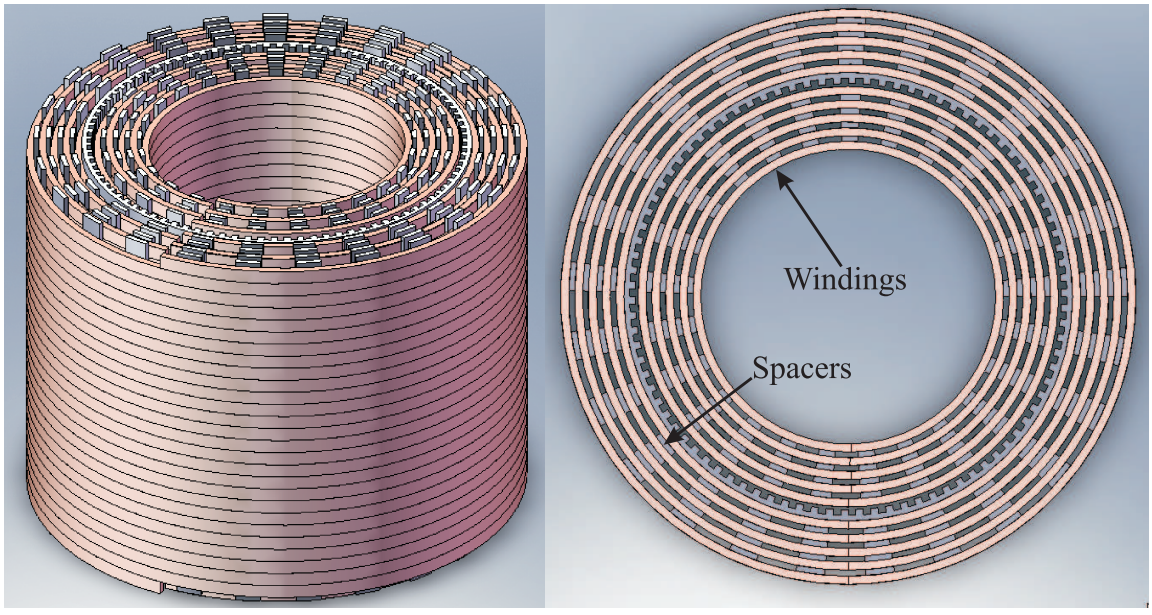

Figure 4.2 Primary and Secondary windings with layer insulation and cooling channels

The transformer is operated at low voltage, hence there is no requirement for much insulation. With the fibreglass spacers and the high electrical breakdown strength of liquid nitrogen, there is no need for additional layer to layer insulation.

The first transformer winding to be built was the copper mockup. The superconductor winding was built after the copper mockup transformer had been tested. Having the same core and winding dimensions, the performance of the two different windings can be compared directly. It is also more convenient to build one core for two different transformers. This also provides a challenge in designing the core so that it can be easily pulled apart and put together.

4.3.1 Material and Design Data

The material of the core is laminated cold rolled grain oriented (CRGO) steel. The decision to pick CRGO was because of its availability at the university. The properties of CRGO steel are listed in table 4.1.

Table 4.1 CRGO steel lamination properties

Lamination thickness	0.23	mm
Density	7650	kg/m^3
Resistivity @ 77K	4.5×10^{-8}	Ω-m
Maximum Flux Density	1.85	T
Maximum Iron Loss	1.00	W/kg

The superconductor tape available at the university was previously used to build the world's first partial core superconducting transformer [5]. The superconducting tape is made out of BSCCO ceramic encased in silver, made by American Superconductors^{TM}. It has a DC critical current of approximately 100A. The other properties of the superconductor tape are listed in table 4.2.

Table 4.2 Superconductor tape properties

Engineering critical current density	79	A/mm^2
Width	4.1	mm
Thickness	0.30	mm
Minimum bend radius	25	mm
Substrate resistivity @ 77K	4×10^{-9}	Ω-m
Wire density	10490	kg/m^3
Critical temperature	108	K
Superconductor material	$Bi_2Sr_2Ca_2Cu_3O_{10}$	

The superconducting tape was manufactured without any electrical insulation. In the previous partial core transformer [5], the tape was insulated with Nitto Nomex^{TM} tape. The Nitto^{TM} tape consists of nylon paper, coated evenly with pressure sensitive adhesive. It is known to withstand cryogenic temperatures with no deterioration of its electrical insulation properties. The tape has a width of 9mm and a thickness of 0.11mm. It also has a breakdown strength of 3.2kV.

The copper tape, which is used in the mock up winding of the superconductor version, was manufactured by Industrial Research Ltd (IRL). The copper tape has a slightly bigger width, because it was designed to be used for growing YBCO superconductor on it. Its dimensions and properties are shown in table 4.3.

Table 4.3 Copper tape properties

Width	4.83	mm
Thickness	0.30	mm
Wire density	8940	kg/m^3
Resistivity @ 77K	1.99×10^{-9}	Ω-m

The core was designed with the intention of minimising its weight as well as the losses. Looking at the power loss equations in chapter 3, the eddy-current power loss can be reduced by having a large cross-sectional area, small effective flux path length and small lamination thickness. The hysteresis loss can be minimised by a process of minimising the core size, i.e. minimising the weight as well as keeping the flux from over saturating the core.

The core design data is shown in table 4.4. Due to the core steps, the actual area of the core is $4.18\times10^{-3}m^2$. This brings the stacking factor to 0.95. However, the laminations were also glued together using polyurethane, effectively reducing the core material. Hence the stacking factor, in table 4.4, was reduced to 0.85. The relative permeability of the core was obtained by matching the model to the equivalent parallel resistance of the open circuit test results, discussed in section 5.

The winding former is made of Tuffnel, a material which consists of epoxy-resin lacquered fabric. This material was tested in liquid nitrogen prior to the design, to observe any shrinkage in diameter and length. However, no significant shrinkage was observed.

Table 4.4 Core design data

Core Dimensions:				
LC	-	Core Length	200.00	mm
WC	-	Core Diameter	75.00	mm
WW	-	Winding Window	41.89	mm
LTC	-	Lamination Thickness	0.23	mm
SFC	-	Stacking Factor	0.85	
IC1	-	Winding Former Thickness	3.25	mm
R20C	-	Resistivity @ 77K	4.5×10^{-8}	Ω-m
URC	-	Relative magnetic permeability	12000.00	H/m
DNC	-	Material Density	7650.00	kg/m^3
OTC	-	Operating Temperature	-196.00	°C

To make the circular core, the laminations were cut and stacked in a stepped fashion. Due to this, the yoke laminations have varying lengths to match the core sections. The full core assembly is shown in figure 4.3. The core laminations are stacked with overlapping adjacent pieces to reduce the effect of air gaps in the core. This is shown in the construction section (chapter 5). As seen in figure 4.3, the limb and the yokes of the transformer are not circular. This makes the limb and yokes easier to construct.

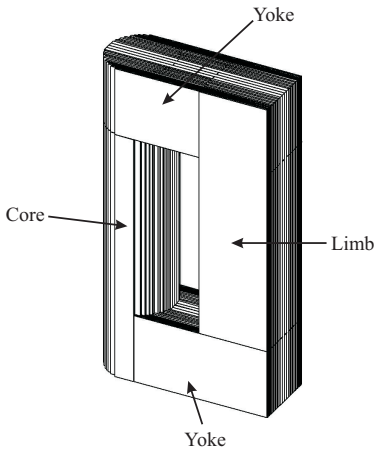

Figure 4.3 Full core assembly

The winding design data is shown in tables 4.5 and 4.6. The priority of the design was to ensure enough cooling of both windings. Working with the materials available in the university, 2mm thick composite fibreglass flat bars were used for the inter-layer insulation. The flat bars were placed with even spaces between each flat bar around each layer. As the number of layers increased, the width of the flat bars was also increased to ensure a firm circular/round winding with no kinks in any of the turns. A graphical construction of the winding (with insulation and winding former) is shown in figure 4.4.

Table 4.5 Copper inside winding design data

Inside winding Dimensions:				
LI	-	Length of inside winding	190.00	mm
L1	-	Number of layers	8	
W1L	-	Wire width	4.83	mm
W1R	-	Wire thickness	0.30	mm
WI1	-	Wire insulation thickness	0.11	mm
I1	-	Insulation layer space	2.00	mm
R201	-	Wire resistivity @ 77K	1.99×10^{-9}	Ω-m
DN1	-	Material density	8940.00	kg/m^3
OT1	-	Operating temperature	77	K

The set of design data for the superconducting winding is presented in tables 4.7

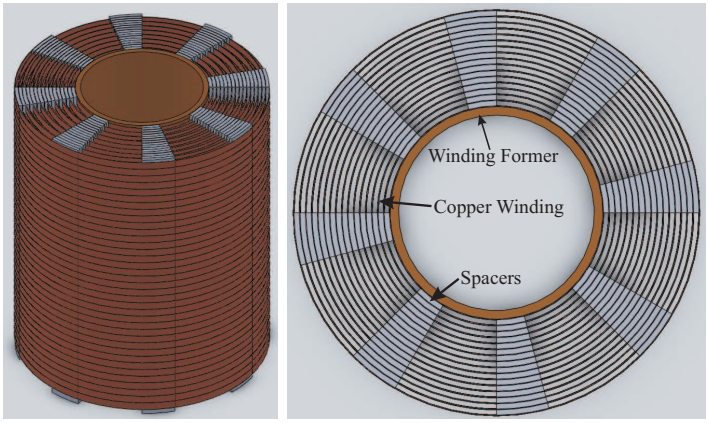

(a) Trimetric view of winding assembly (b) Top view of winding assembly

Figure 4.4 Winding assembly

Table 4.6 Copper outside winding design data

Copper outside winding Dimensions:				
LO	-	Length of outside winding	190.00	mm
L2	-	Number of layers	8	
W2L	-	Wire width	4.83	mm
W2R	-	Wire thickness	0.30	mm
WI2	-	Wire insulation thickness	0.11	mm
I2	-	Insulation layer space	2.00	mm
R202	-	Wire resistivity @ 77K	1.99×10^{-9}	Ω-m
DN2	-	Material density	8940.00	kg/m^3
OT2	-	Operating temperature	77	K

Table 4.7 Superconducting inside winding design data

Superconducting inside winding Dimensions:				
LI	-	Length of inside winding	190.00	mm
L1	-	Number of layers	8	
W1L	-	Wire width	4.10	mm
W1R	-	Wire thickness	0.30	mm
WI1	-	Wire insulation thickness	0.11	mm
I1	-	Insulation layer space	2.00	mm
R771	-	Substrate resistivity @ 77K	4.00×10^{-9}	Ω-m
DN1	-	Material density	10490.00	kg/m^3
OT1	-	Operating temperature	77.00	K

and 4.8. The spacers and insulation design of the superconducting winding is the same as the copper mockup. The main difference is the wire width, which is 0.73mm less than the copper tape. However this winding still had the same number of turns as the copper version. The substrate resistivities, R771 and R772, shown in tables 4.7 and 4.8,

Table 4.8 Superconducting outside winding design data

Superconducting outside winding Dimensions:				
LO	-	Length of outside winding	190.00	mm
L2	-	Number of layers	8	
W2L	-	Wire width	4.10	mm
W2R	-	Wire thickness	0.30	mm
WI2	-	Wire insulation thickness	0.11	mm
I2	-	Insulation layer space	2.00	mm
R772	-	Substrate resistivity @ 77K	4.00×10^{-9}	Ω-m
DN2	-	Material density	10490.00	kg/m^3
OT2	-	Operating temperature	77.00	K

are not directly used to calculate the resistance of the superconductor. These are used in the calculations for the eddy current losses in the silver matrix which contribute to part of the total resistance of the superconductor.

Figure 4.5 shows the full transformer assembly, which consists of the spacers, windings and core.

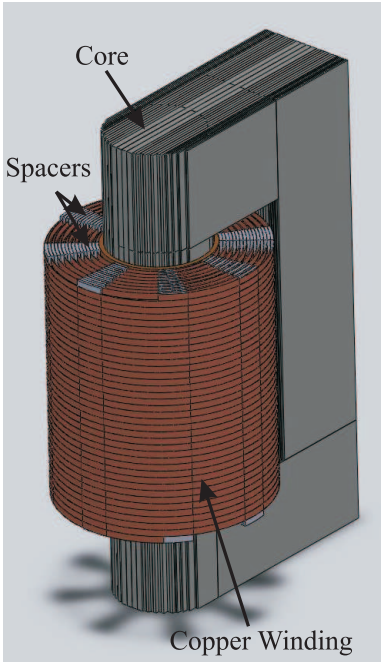

Figure 4.5 Full transformer CAD

4.3.2 Copper Transformer Model Simulation

The transformer model was simulated in MATLAB© using the equations described in chapter 3. The first result is the calculated parameters of the core, which is shown in table 4.9.

Table 4.9 Core design calculations

Core Parameters:				
V1	-	Applied primary voltage(inside winding)	230.00	V
BA	-	Aspect ratio	4.92	
NLC	-	Number of core laminations	277	
PC	-	Operating resistivity	4.50×10^{-8}	Ω-m
EC	-	Penetration depth	0.14	mm
CR	-	Core reluctance	13841	H^{-1}
AC	-	Core cross sectional area	4418	mm^2
EAC	-	Effective core area	3755	mm^2
BMC	-	Maximum flux density	0.93	T
VOC	-	Total core volume	2.94×10^{-3}	m^3
WTC	-	Total core weight	22.52	kg

The core model suggests that even at cryogenic temperatures, the skin depth is still large enough that the eddy currents are creating a uniform flux distribution in the core. The winding dimension calculations are shown in table 4.10.

Table 4.10 Copper winding design calculations

Inside Winding Parameters:				
N1	-	Number of turns	296	
P1	-	Operating resistivity	1.99×10^{-9}	Ω-m
EC1	-	Skin depth	3.18	mm
LE1	-	Length of conductor	91.55	m
WI	-	Outside width	118.14	mm
VO1	-	Winding volume	1.09×10^{-3}	m^3
VW1	-	Wire volume	1.33×10^{-4}	m^3
PF1	-	Packing factor	0.12	
WT1	-	Weight of conductor	1.19	kg
Outside Winding Parameters:				
N2	-	Number of turns	296	
P2	-	Operating resistivity	1.99×10^{-9}	Ω-m
EC2	-	Skin depth	3.18	mm
LE2	-	Length of conductor	125.62	m
WO	-	Outside width	160.78	mm
VO2	-	Winding volume	1.53×10^{-3}	m^3
VW2	-	Wire volume	1.82×10^{-4}	m^3
PF2	-	Packing factor	0.12	
WT2	-	Weight of conductor	1.63	kg

Table 4.11 shows the equivalent circuit parameters in the Steinmetz model. The hysteresis loss resistance is less than the eddy current resistance and hence the hysteresis losses will be larger than the eddy current losses (as expected from chapter 3). R_1 has

a lower resistance than R_2 due to the outside winding having a longer length.

Table 4.11 Equivalent Steinmetz circuit equivalent circuit parameters:

Core parameters				
REC	-	Core eddy current resistance	4290.00	Ω
RH	-	Hysteresis resistance	2228.41	Ω
RC	-	Total core resistance	1466.02	Ω
XM	-	Magnetising reactance	1988.66	Ω

Winding parameters				
R1	-	Inside winding resistance	0.126	Ω
X1	-	Inside winding reactance	0.482	Ω
R2	-	Outside winding resistance	0.173	Ω
X2	-	Outside winding reactance	0.482	Ω

With all the Steinmetz equivalent circuit parameters calculated, a full performance simulation was undertaken to see how well the transformer operates. This included open-circuit, short circuit and full load simulations. The results of the simulations are shown in tables 4.12, 4.13 and 4.14.

The open circuit simulation (table 4.12) shows that the core does not have a very high magnetising current as compared to the transformer rated current, as expected of full core transformers. The simulation shows a secondary voltage of 229.95 volts which indicates almost perfect coupling of the flux between the primary and secondary windings. The indicated power loss of the core is 36W.

The short circuit simulation (table 4.13) shows significant winding losses at a 65A current. The secondary winding is simulated to have more winding losses, which is to be expected since it has a longer tape length. The apparent power is much higher than the real power component which indicates that it is very inductive in nature, reflective of the leakage reactances being higher than the winding resistances.

The loaded circuit performance (table 4.14) was evaluated by simulating a nominal 15kW load attached on the outside (secondary) winding, which equates to having a 3.53Ω resistor at the rated 230V. The losses in the transformer are not taken into account in determining the load resistance. The real power transferred to the load is less than 15kW, as shown in the simulation, because the transformer is operating at 91.9% efficiency. Most of the losses are in the windings (96% of the total losses).

Table 4.15 shows the voltages of the transformer under full-load conditions. The secondary voltage was simulated to be 205.5V resulting in 10.6% voltage regulation. The Nitto^{TM}insulation tape has more than enough insulation for the required turn to turn voltage of 0.8V. The liquid nitrogen and fibreglass spacers also have much higher voltage breakdown strength than the required breakdown voltages of the winding layers (ranging from 51.3V to 57.5V).

Table 4.12 Open Circuit performance calculations

Open circuit performance				
VOC	-	Applied open circuit voltage (inside winding)	230	V
V2O	-	Secondary voltage	229.95	V
IO	-	Magnetising current	0.19	A
SO	-	Apparent power	44.80	VA
PO	-	Real power	36.10	W
PFO	-	Power factor	0.81	
RO	-	Equivalent parallel resistance	1466.79	Ω
XO	-	Equivalent parallel reactance	1988.60	Ω
P1	-	Inside winding real power	4.79×10^{-3}	W
P2	-	Outside winding real power	0	W
PC	-	Core real power	36.10	W

Table 4.13 Short Circuit performance calculations

Short circuit performance				
VS	-	Applied short circuit voltage (inside winding)	65.50	V
II	-	Inside winding current	64.95	A
IOS	-	Outside winding current	64.92	A
SS	-	Apparent power	4.25	kVA
PS	-	Real power	1.26	kW
PFS	-	Power factor	0.29	
RS	-	Equivalent series resistance	0.30	Ω
XS	-	Equivalent series reactance	0.96	Ω
P1	-	Inside winding real power	532.91	W
P2	-	Outside winding real power	730.68	W
PC	-	Core real power	0.70	W

4.4 CONSTRUCTION

The construction of the transformer started with the steel core, where the steel laminations needed to be cut to different lengths and widths. The steel laminations were cut using an air compressor guillotine. They were then stacked in groups of ten and glued together with poly-urethane.

The next phase of the project was to insulate the copper tapes. An insulating device, built for the partial core superconducting transformer [5], was used to insulate the copper tape. The insulating machine folded two separate lengths of Nitto^{TM} tape onto the copper while it was extruded through the machine. This process is described in subsection 4.4.2. After insulating, the tape was wound onto the winding former. After the first layer was wound, the spacers were placed on top of the first layer, and the second layer was wound onto the spacers. This process was repeated until eight layers were wound for the inside winding. The same was done for the outside winding.

Table 4.14 Loaded Circuit performance calculations

Loaded circuit performance				
RL	-	Load resistance	3.53	Ω
VL	-	Applied loaded voltage (inside winding)	230.00	V
IS	-	Inside winding current	58.43	A
J1	-	Inside winding current density	40.33	A/mm^2
IO	-	Outside winding current	58.27	A
J2	-	Outside winding current density	40.21	A/mm^2
S1	-	Inside winding apparent power	13.44	kVA
P1	-	Inside winding real power	13.03	kW
S2	-	Outside winding apparent power	11.97	kVA
P2	-	Outside winding real power	11.97	kVA
RSL	-	Equivalent series resistance	3.82	Ω
XSL	-	Equivalent series reactance	0.97	Ω
EFF	-	Efficiency	91.92	%

Table 4.15 Voltage insulation calculations (loaded circuit conditions)

Loaded circuit voltages				
VT1	-	Inside winding voltage per turn	0.78	V
VL1	-	Inside winding voltage per insulation layer	57.50	V
EL1	-	Inside winding insulation layer voltage gradient	28.70	V/mm
VE1	-	Internal voltage, referred to inside winding	217.42	V
V2	-	Outside winding terminal voltage	205.50	V
VT2	-	Outside winding voltage per turn	0.69	V
VL2	-	Outside winding voltage per insulation layer	51.38	V
EL2	-	Outside winding insulation layer voltage gradient	25.70	V/mm
VTR	-	Outside/inside terminal voltage ratio	0.89	
VREG	-	Voltage regulation	10.65	%

The final layer on the outside winding was bound with Scotch^{TM} tape to keep the layer from unravelling.

The next step was to assemble the entire core together with the windings. As mentioned previously, the glued laminations were stacked alternately, overlapping the adjacent pieces of the glued laminations. The process is described in subsection 4.4.1.

The core steel was fastened with four pieces of C-shaped steel bars. Two of the steel bars were used to tighten the steel core on the top limb and two on the bottom limb. This is common practise for holding steel cores together in conventional transformers. After this, a flat piece of Tuffnel was fitted on top of the C-shaped steel bars. Terminals were then bolted onto the Tuffnel piece and the ends of the copper winding bolted onto the terminals.

The transformer was then tested under open circuit, short circuit and loaded circuit conditions operating at both liquid nitrogen and room temperatures. If the transformer operated without failing due to an unforseen design fault, the superconducting winding was to be built. This proved to be the case.

The process of insulating the superconducting tape was the same as for the copper tape. During the process, the tape was extruded through the machine very slowly to avoid bending. After insulating, the superconductor tape was wound around another winding former in the same fashion as for the copper winding.

To finish building the superconducting windings, the ends of the windings were terminated. To do this, long strips of thick copper pieces were soldered (with low temperature melting solder) on to the superconducting windings. The copper pieces were then bent to shape so that they could be bolted onto the terminals.

4.4.1 Steel Laminated Core

The steel laminations of the core were required to be cut into different lengths. The dimensions for the central core piece and lengths of the limb laminations are shown in Figure 4.6.

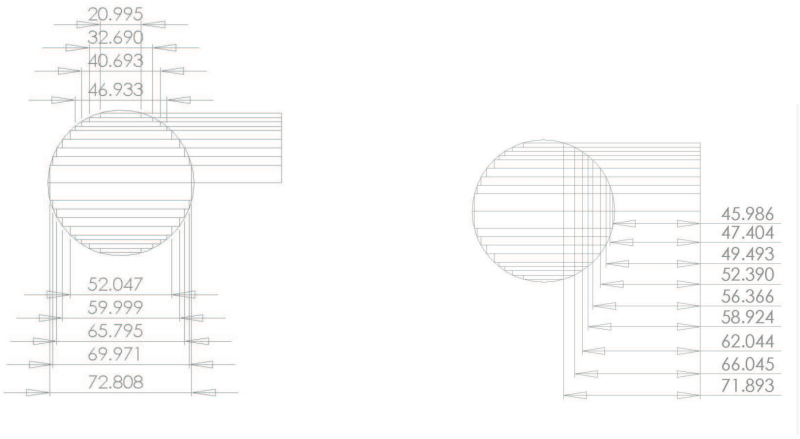

(a) Dimensions of stepped core in mm

(b) Dimensions of the limb laminations in mm

Figure 4.6 Core lamination dimensions for the circular core section and limb sections

After cutting, the laminations were glued in stacks of ten. These stacks were placed with other stacks to overlap the air gaps in between connecting layers. This is shown in figure 4.7, where figure 4.7(a) can be stacked side by side with figure 4.7(b) to overlap the air gaps.

Figure 4.8 shows the finished core middle section laminations cut but not fully assembled with the limbs and yoke. Figure 4.9 shows the finished laminations of the limbs and yoke.

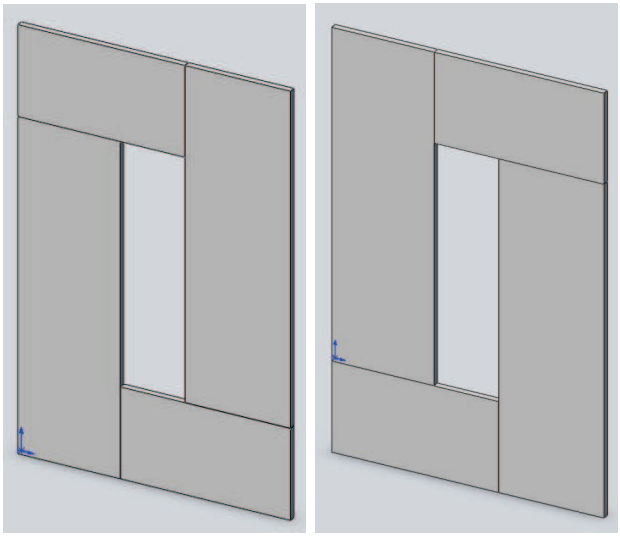

(a) "Anticlockwise laminations" (b) "Clockwise laminations"

Figure 4.7 Different stacks of laminations which can be placed on top of each other to overlap the air gaps

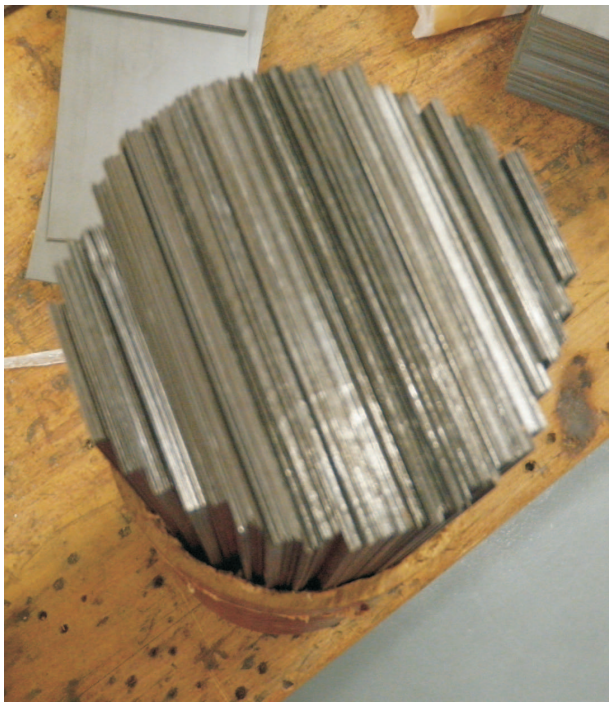

Figure 4.8 Core mid section laminations

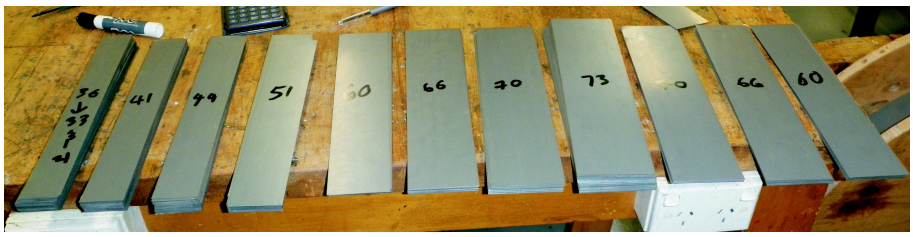

Figure 4.9 Finished lamination cuts

The partially completed yoke and limbs are shown in figure 4.10, the glued laminations are stacked on top of each other in the alternating order described before. To assemble the whole transformer, the windings were placed in between the two limbs. The middle core section laminations were placed through the gaps of the limb laminations and through the winding former.

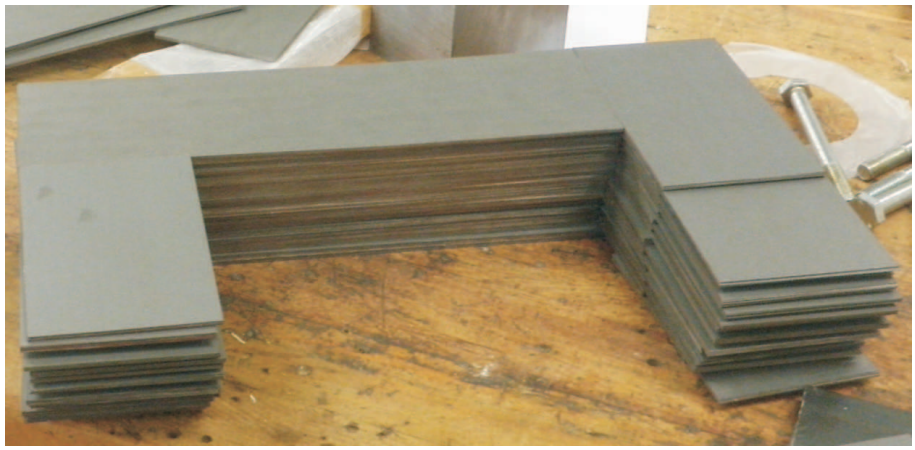

Figure 4.10 Partially constructed core, limbs and yoke

The steel fasteners of the core are shown in figure 4.11. The steel fasteners were not shown in the SolidWorks^{TM}full assembly (figure 4.5) but are necessary components to hold the core together. The steel fasteners were sand-blasted and galvanised to prevent rusting. The reason steel was chosen was because it will have the same coefficient of contraction as the core. When the transformer is operated at liquid nitrogen, the steel core will still be held together by the fasteners. The steel fasteners are held and tightened with four 100mm bolts and nuts per pair of fasteners. Due to the materials used for the fasteners, there could be eddy currents flowing in them. It would be better to use a non-metallic material. However, it is hard to find a material that would contract at the same rate of steel at low temperatures. Most of the flux should flow through the core, and there should not be much stray flux outside of the core.

Figure 4.11 Steel Fasteners

4.4.2 Copper Winding

Figure 4.12 shows the machine that insulates the copper tape. The copper tape was fed through rollers and two reels of Nitto^{TM} tape were folded over the bare copper. The folding action is done by a "folding device" that folds half of the tape onto each side of the copper tape. The Nitto^{TM} tape has a width that is twice the width of the copper tape. There are two of these "folding devices" in the insulating machine, so that all sides of the copper tape are insulated by the Nitto^{TM} tape. Figure 4.13 shows the process in more detail.

Figure 4.12 Insulating machine

Figure 4.14 shows the completed inside winding. As mentioned before, the fibreglass composite spacers are placed at regular intervals around the windings. The disadvantage of this design is that the copper winding in contact with the spacers will

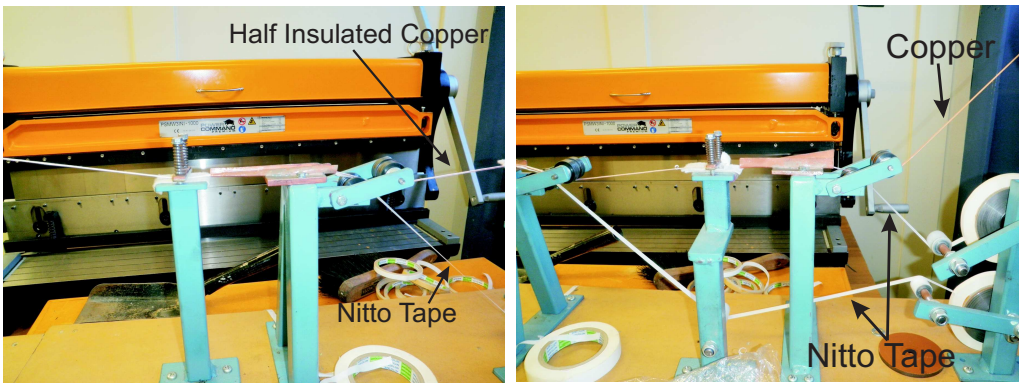

(a) Insulating the one side of the copper tape (b) Copper tape feed and insulating the other side of the copper tape

Figure 4.13 Insulation process of the copper tape

have less exposure to liquid nitrogen. An improvement to the cooling channels could be to have fibreglass rods replace the spacers.

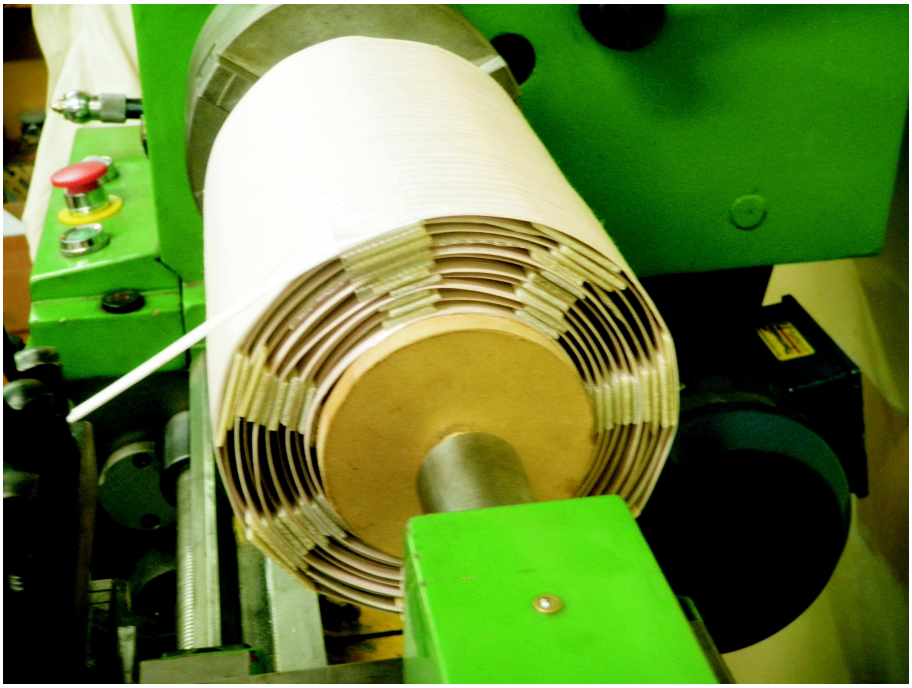

Figure 4.14 Copper inside winding on lathe with composite fibreglass spacers

4.4.3 Full Assembly

Figure 4.15 shows the full transformer assembly. The pieces of paper sicking out in between the core limbs and the windings are Nomex-Mylar-Nomex^{TM} insulation. This is to prevent the core laminations cutting through the winding insulation and shorting out the windings to ground (the core).

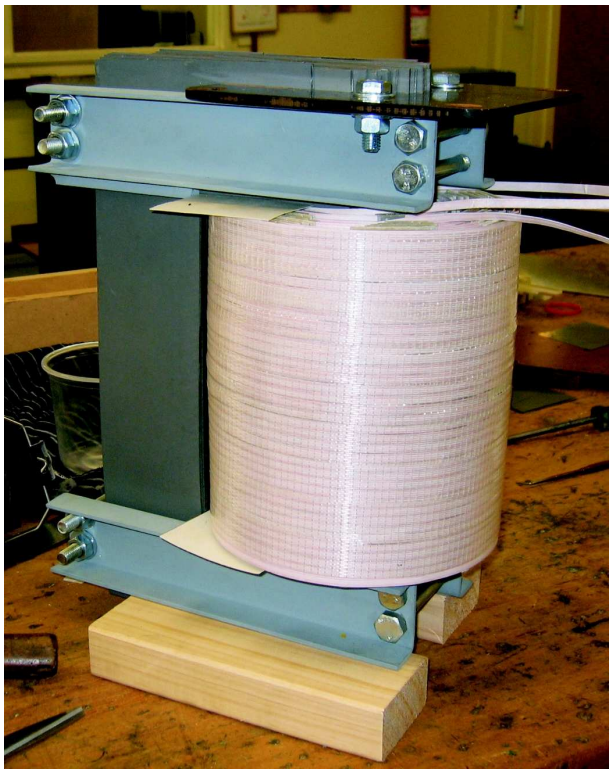

Figure 4.15 Full transformer assembly

To test the mechanical integrity of the full transformer, the assembly was submerged in liquid nitrogen. Figure 4.16 shows the transformer during the filling. This coincided with some electrical testing, discussed in chapter 5. The transformer was submerged in liquid nitrogen for more than two hours (including filling time). The transformer was taken out the next day to note any mechanical strain or damage to the assembly. There was no visible damage and the whole assembly was still intact when taken out of the dewar.

Nothing mechanical failed or cracked due to contraction at the liquid nitrogen temperature. There were no visible kinks or bends in the copper tape, indicating that this design would be suitable for the superconducting winding. The copper mockup transformer testing was thus a success in terms of the mechanical design.

4.4.4 Superconducting Transformer

The superconducting windings were built the same way as the copper mockup. The superconducting tape was also insulated using the insulating machine shown in figure 4.12. The machine needed to be reconfigured to make sure that the guides would not bend the tape past the rated bending radius.

After insulation, the superconducting tape was wound onto a winding former using the winding machine. Spacers were then placed on top of the first layer of windings. The

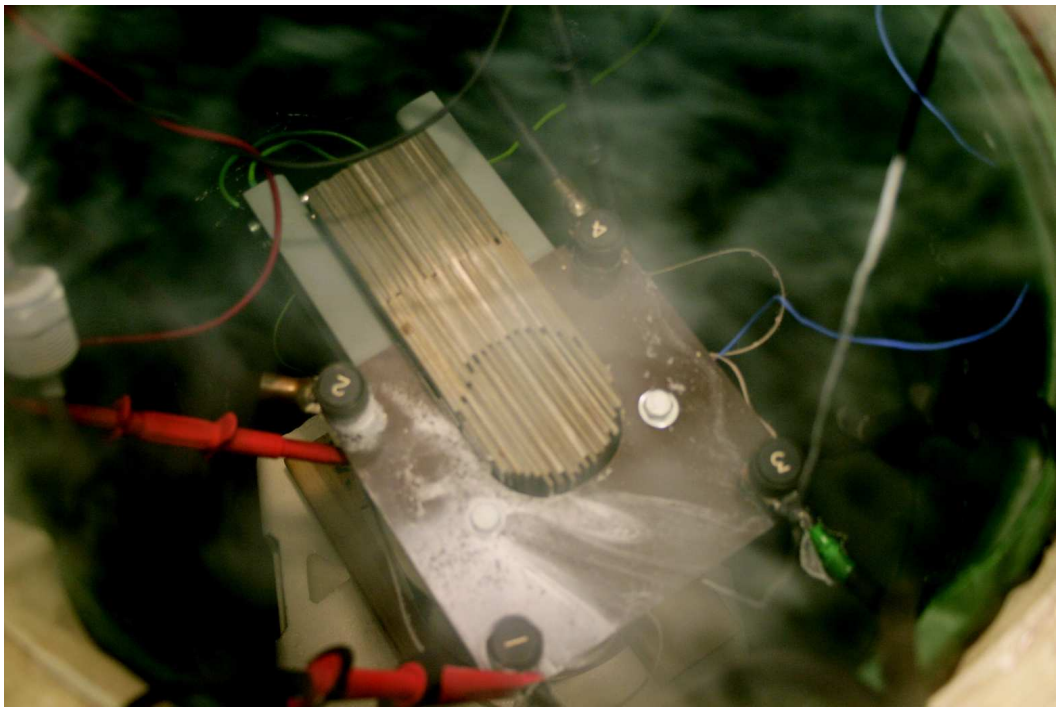

Figure 4.16 Copper transformer under liquid nitrogen conditions

second layer of windings were wound on top of the spacers and this was repeated until the inside and outside windings were completed. The last layer of the outside winding was bound with Scotch^{TM} tape to prevent the outside winding from unraveling. A K-type thermocouple was also embedded into the middle of the last layer of the inside winding to monitor the temperature. The test results of the copper mockup transformer showed that the outside winding voltage, under full load conditions, was unsatisfactory (189V). Extra turns were added to the outside winding to compensate for this.

4.4.4.1 Copper Terminations

The superconductor tape ends were terminated with long pieces of copper strips. The idea was to prevent the ends of the superconductor from moving and bending. At the superconductor winding ends, the spacers were slightly displaced so the copper terminations would fit into the windings. To keep the termination resistance to a minimum, two pieces of copper strip were used, one on each side of the superconductor tape. It was recommended by the American Superconductor© data sheet that low melting temperature solder is used for any splicing or joins of the superconducting tape. The reason for this is to keep the steel of the superconductor tape from delaminating. The solder used was made out of 97% indium and 3% silver, with a melting temperature of 120°C. The flux used was called Ersin red jelly flux paste. A soldering iron with a large thermal mass was used. This is to keep the temperature from dropping excessively

when touching the soldering iron onto the copper strips and superconductor. The soldering iron temperature was monitored using a K-Type temperature probe and controlled using a variable AC power source.

The copper strips were bent so that they curved around where the superconductor tape ends. First, the copper strips were tinned with the solder on the sides that were going to be in direct contact with the superconductor tape. The flux paste was then applied onto the superconductor and the tinned sides of the copper strips. The copper strips were then clamped lightly together with the superconductor tape in between them. Initially, the Ersin flux was applied to the copper strips to remove oxidisation. Then the soldering iron was gently touched on the two copper strips and more flux was applied to conduct heat throughout the surface of the copper strips. Figure 4.17 shows the terminations on the inside and outside windings. The copper strips were then bolted onto the fixed terminals on a Tuffnel plate (figure 4.18).

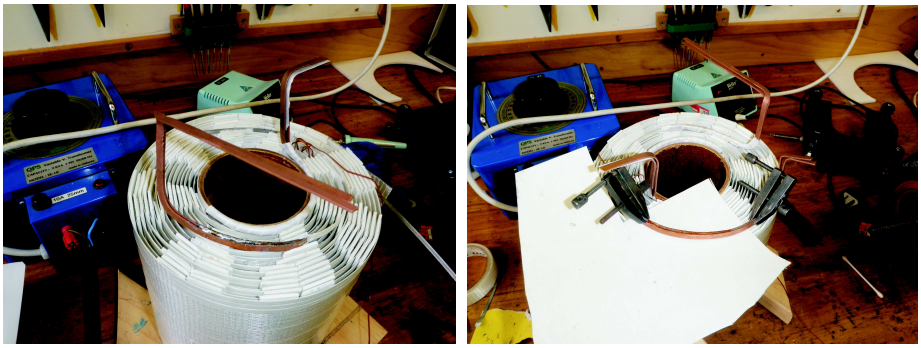

(a) Inside winding terminations (b) Outside winding termination

Figure 4.17 Copper terminations on the ends of the superconductor winding

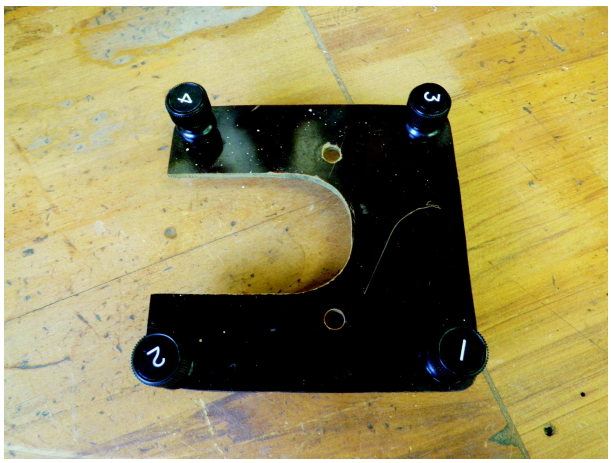

Figure 4.18 Tuffnel plate with fixed terminals, terminals 1 - 2 for inside winding connections and terminals 3 - 4 for outside winding connections.

4.4.4.2 Transformer Assembly

The next step was to assemble the core lamination stacks. They were arranged in the same way as for the copper transformer except that the top limb was fitted in last. Figure 4.19 shows the semi-assembled core. With this arrangement, the windings were slid onto the middle core section through the top. Finally, the top limb lamination stacks were placed and fastened with the steel fasteners. Figure 4.20 shows the full superconducting transformer assembly.

Figure 4.19 The steel core assembly without the top limb assembled.

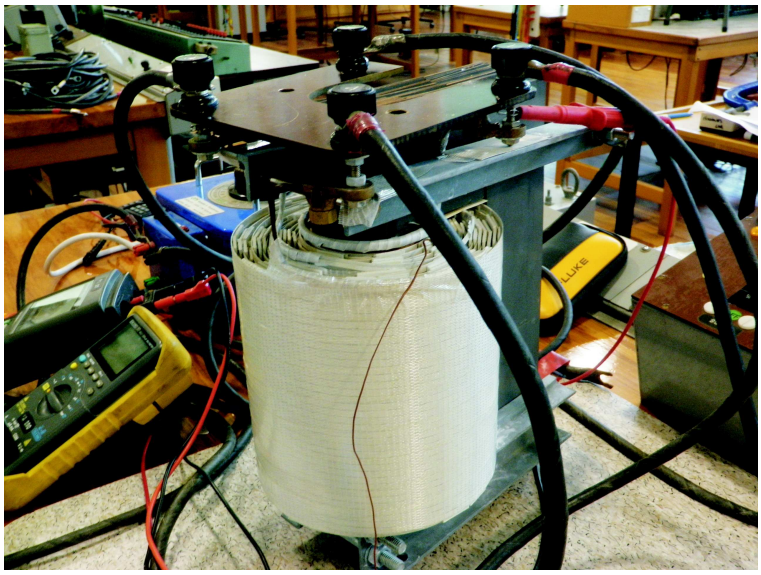

Figure 4.20 Full superconducting transformer assembly

4.5 CONCLUSION

The design and construction of both the copper mockup and superconducting transformer were presented. The design issues were discussed and the transformer was designed to overcome these issues. A proposed winding container was presented, however manufacturing the container was deemed to be too expensive for the project.

Next, a new cooling design for the windings was proposed to overcome the problems experienced in the previous partial core superconducting transformer [5]. Fibreglass rectangular bars were used and placed at regular intervals around each layer.

The design of the transformer core was described first, the materials used and their properties were presented. The objective was to build a transformer core that would be easily taken apart and put together. The core was designed to minimise power loss, so the core would be a minor contributor to liquid nitrogen boil-off.

The copper mockup transformer design was then simulated under open circuit, short circuit and full load conditions. The results show that the core dissipated 36W at nominal voltage and that there were 1.2kW of losses in the windings under short circuit conditions. The full load simulation indicated an efficiency of 91.92%. The simulation of the superconductor tape performance is discussed in chapter 5.

Finally, the construction of both transformers was described. The process of cutting the core laminations and assembling the core was presented. Additional features of the transformer (that were not shown in the CAD), such as the steel fasteners and the terminal plate, were described. The process of insulating the copper tape was shown, the same process was used for insulating the superconducting tape. The ends of the superconducting winding were terminated using copper strips. Low temperature solder and red jelly flux paste were used to solder the copper strips onto the ends of the windings. The final assemblies of the copper mockup and superconducting transformers were shown.

Chapter 5

TESTING, RESULTS AND DISCUSSION

5.1 INTRODUCTION

The testing methodology of the copper mock up transformer and superconducting transformer is described. The tests performed were open circuit, short circuit and various load tests. These were performed in both liquid nitrogen and at room temperature. The findings of the tests are presented and discussed. The simulated model results are then compared with the test results. Anomalies in the model were observed and corrections were implemented. The changes from the corrections and the impact of these on the reactance model theory are discussed.

5.2 TESTING METHODOLOGY

The container used for the testing was a double skinned insulated dewar (shown in figure 5.1). It is made out of two buckets, where one bucket is smaller and fits inside the other. The walls between the smaller bucket and the larger bucket is filled with thermal insulation. The top of the dewar is covered with a thick piece of polystyrene. This container is not ideal for long term operation, as its thermal insulation is not very efficient at keeping heat from the ambient air from heating the liquid nitrogen.

5.2.1 Copper Mock Up Transformer Testing Methodology

Resistance tests were undertaken on the copper mock up transformer (CTX). Measurements were taken on the inside winding and outside winding, prior to, during and after liquid nitrogen submersion. The before and after submersion tests determine whether the submersion has caused any damage to the windings and joins to the terminals. The temperature was also recorded during these tests.

Next, the CTX was tested under open circuit, short circuit and full load conditions, operating at liquid nitrogen temperature. The open circuit test was performed by applying 230V on the inside winding. The readings were measured using two Fluke®41

Figure 5.1 The dewar used for testing the CTM and SCTX in LN2

meters. The Fluke®41 meters were calibrated and had their batteries changed prior to testing.

The short circuit test involved shorting the outside winding and applying voltage on the inside winding until 30A was flowing through the inside winding. This test was performed for one minute.

The loaded circuit test was performed at 230V and 11.3kVA load with a power factor of 0.97. This is equivalent to about 50A flowing in the inside winding. This test was performed for less than two minutes, as it is destructive and could potentially cause damage to the transformer.

The CTX was also tested at room temperatures. These were open circuit, short circuit and a 10A load tests. The open circuit test was performed at 230V with the inside winding energised. The short circuit test was performed with the outside winding shorted and 20A flowing in the primary winding.

During the CTX tests, temperatures in the windings were monitored using K-type thermocouples, with their tips attached to different parts of the windings.

5.2.2 Superconducting Transformer Testing Methodology

The superconducting transformer (SCTX) was tested under liquid nitrogen and at room temperature. The transformer was subjected to open circuit, short circuit and loaded tests, where all these tests were performed for a duration of 2 minutes or more. The duration of the tests, upon successful testing, reinforce whether cooling was the problem experienced in the previous partial core superconducting transformer.

Before testing began, the transformer was "prepared" to minimise the risk of quenching the superconductor. Due to the terminal bolts being made out of different materials, the connections may come loose as the bolts will contract at different rates at low temperature. This will cause a high resistance connection and may heat up the superconducting winding hence quenching the superconductor. To minimise this risk, the bolts were tightened as much as possible and resistance tests were performed prior to each testing. There is also the risk that the cable leads, connected to the transformer terminals, might conduct enough heat to quench the superconductor. The cable leads that were used had large cross-sectional areas and were three to five meters in length. Most of the cable was coiled up and submerged together with the transformer. This was so that most of the cable was at thermal equilibrium with the liquid nitrogen and creates a thermal buffer between the outside environment and the superconductor. This would mean it would require more energy (from the environment) to increase the temperature of the transformer winding system. Considering only heat conduction in 1 dimensional space, the equation that governs heat conduction is shown in equation 5.1.

$$\frac{Q}{t} = \frac{kA(\Delta T)}{d} \quad (W) \tag{5.1}$$

where,

Q	=	Heat conduction energy	(J)
t	=	Time	(s)
k	=	Thermal conductivity	(W/m°C)
A	=	Cross sectional (or surface) area	(m^2)
ΔT	=	Temperature difference between two surfaces	(°C)
d	=	Distance between the two surfaces	(m)

By increasing the the length of the cable, the heat conduction loss is decreased. However, the I^2R losses of the cable must be taken into account as well due to the resistance linearly increasing with length. Assuming that the cross sectional area of the cable is kept constant, the optimal cable lead length can be found as shown in Figure 5.2.2. However, it was difficult to determine the thermal conductivity of the combination of copper conductor and its insulation hence the calculation was not carried out. Furthermore, a 300A cable lead was used for a maximum supply of 65A (for this experiment) hence the I^2R losses should not dominate. A 5m length was used as

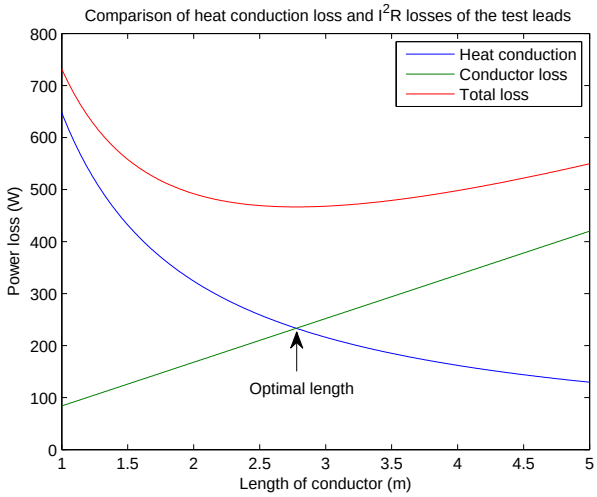

Figure 5.2 Comparison of the heat conduction losses and the I^2R losses of the cable leads

it was deemed sufficient to overcome the heat conduction losses at the time for these experiments.

The transformer was submerged for an hour before any tests began. This was to ensure that the whole transformer was completely cooled down.

The first test was the resistance test. The test was performed before, during and after submerging the transformer in liquid nitrogen. The test equipment used was a digital micro-ohm meter which calculates the resistance based on a Wheatstone bridge configuration. The resistance was checked after every other test in liquid nitrogen, to ensure the winding was still superconducting.

The SCTX was tested under open circuit conditions. The voltage applied was 230V on the inside winding. The Fluke®41 meters were set up so that all the harmonics up to the 40^{th} harmonic was recorded. This was so that a complete voltage and current waveform could be reconstructed, based on these harmonics, with Fourier equations.

The next test was the short circuit test undertaken for a 2 minute duration. This was performed with the outside winding of the transformer shorted. The voltage applied on the inside winding was slowly increased until 40A was passing through the inside winding. The temperature of the winding was monitored throughout the test.

The loaded tests were performed with increasing unity power factor loads, starting from 10A to 60A, in steps of 10A. The resistive loads were connected to the outside winding. Each of these tests was performed for 2 minutes, except for the 60A loaded test which was performed for 3 minutes. Again, the duration of the test determined if the cooling channels worked. The temperatures in the windings were monitored throughout all these tests. The rate of liquid nitrogen boil off was also observed in each of these tests.

5.3 COPPER MOCK UP TRANSFORMER

5.3.1 Test Results

Tables 5.1 to 5.3 show the tests done on the CTX operated at liquid nitrogen (LN2) temperature. The winding temperature remained constant throughout all these tests and was measured to be −6.5mV (at the terminals of the K-type temperature probe). This value corresponds to the temperature of boiling LN2 or −196°C. The reason a direct voltage measurement was taken on the terminals of the K-type temperature probe was because the thermocouple converter was not linear below −50°C. There was no significant LN2 boil off for the open circuit test. The rate of LN2 boil off rapidly increased during the short circuit and full load tests. Although the original intention was to run the transformer at full load for more than 2 minutes, the full load test was cut short. The rate of LN2 boil off was causing part of the transformer to be exposed to open air. This was deemed unsafe for the transformer at the time.

Table 5.1 CTX Open circuit test results, operated at liquid nitrogen temperature

Open circuit test		
Primary voltage	230	V
Primary current	0.12	A
Primary real power	19	W
Primary apparent power	28	VA
Primary power factor	0.7	
Secondary voltage	226	V
Voltage ratio	0.99	

Table 5.2 CTX Short circuit test results, operated at liquid nitrogen temperature

Short circuit test		
Primary voltage	35.3	V
Primary current	30.6	A
Primary real power	410	W
Primary apparent power	1080	VA
Primary power factor	0.38	
Secondary current	30.9	A
Current ratio	1.01	

The CTX was taken out for visual inspection after the LN2 tests. There was no visible damage on the winding or the core. The core became significantly rusty due to the moisture build up during the “defrosting” period. Figure 5.3 shows the transformer during the “defrosting” period.

Table 5.3 CTX Full load test results operated at liquid nitrogen temperature

Full load test					
Primary voltage	229	V	Secondary voltage	189	V
Primary current	49.3	A	Secondary current	49	A
Primary real power	10.2	kW	Secondary real power	9	kW
Primary apparent power	11.3	kVA	Secondary apparent power	9.3	kVA
Primary power factor	0.9		Secondary power factor	0.97	
Efficiency	88.23	%			
Voltage regulation	15.8	%			

Figure 5.3 Frozen transformer and leads

Tables 5.4 to 5.6 show the CTX tests at room temperature. During the open circuit test, there was no observable increase in temperature of the windings. In the short circuit test, the temperature of the inside windings rose to about 60°C and the temperature of the outside windings rose to about 30°C within a minute. The 10A endurance test was performed for 5 minutes. The temperature of the inside windings rose to 45.4°C and 29.4°C for the outside winding. The room temperature was 17.6°C on the day of testing.

Table 5.6 shows that the transformer is slightly capacitive in nature due to the primary winding power factor being slightly higher than the secondary winding. However, it is suspected that the resolution of the meter used is not adequate.

5.3.2 Discussion

The open circuit test at LN2 temperature (table 5.1) shows near perfect coupling between the inside and outside windings. The magnetising current is small, typical of full core transformers. The power loss in the core is 19W which was lower than

Table 5.4 CTX Open circuit test results, operated at room temperature

Open circuit test		
Primary voltage	230	V
Primary current	0.13	A
Primary real power	16	W
Primary apparent power	29	VA
Primary power factor	0.57	
Secondary voltage	227	V
Voltage ratio	1.02	

Table 5.5 CTX Short circuit test results, operated at room temperature

Short circuit test		
Primary voltage	60.5	V
Primary current	19.2	A
Primary real power	1.1	kW
Primary apparent power	1.16	kVA
Primary power factor	0.95	
Secondary current	18.9	A
Current ratio	1.02	

Table 5.6 CTX 10A endurance test results operated at room temperature

10A endurance test					
Primary voltage	228	V	Secondary voltage	195	V
Primary current	9.96	A	Secondary current	9.55	A
Primary real power	2.27	kW	Secondary real power	1.86	kW
Primary apparent power	2.27	kVA	Secondary apparent power	1.87	kVA
Primary power factor	1.00		Secondary power factor	0.99	
Efficiency	81.62	%			
Voltage regulation	13.34	%			

anticipated in the model (36W). This may be due to the resistivity of steel being set to $4.5\times10^{-8}\Omega m$ in the model (chapter 3). This value might be inaccurate and might need to be revised.

The short circuit test results at LN2 temperature (table 5.2) show conflicting numbers when compared with the simulated results (table 4.13). The real power measured (410W) in the windings was higher than indicated in the model (370W). The slight difference in the real power can be caused by several factors. The resistivity (equation 3.3) in the model could be incorrect. Also the cable shorting the secondary was at room

temperature and should be considered as a low resistance. However, it is modelled as a perfect short circuit (0Ω) in the simulation.

Table 5.7 Comparison between the copper mock up transformer test results and the model, operating at liquid nitrogen temperature

	Test results		Model		
Winding	Inside	Outside	Inside	Outside	
Voltage	229	189	230	210.28	V
Current	49.3	49	49.29	49.13	A
Real power	10.2	9	11.09	10.33	kW
Apparent power	11.3	9.3	11.34	10.33	kVA
Power Factor	0.9	0.97	0.978	1	
Phase	25.84	14.07	12.04	0	
ESR	4.197	-	4.565	-	Ω
ESL	2.026	-	0.973	-	Ω
Efficiency		88.24		93.15	%
Voltage Regulation		15.8		10.4	%

Table 5.7 gives a comparison between the test and the model results. ESR and ESL are the equivalent series resistance and the equivalent series reactance, respectively. The test result ESL is higher than the model ESL. This indicates that the reactance calculations in the model is incorrect. Further discussion about the ESL and a possible correction to the model is described section 5.4.2.

The open circuit test at room temperature showed that the core had slightly less core losses (16W) compared to operating at liquid nitrogen (19W). The small increase in core losses is expected (discussed in chapter 4).

The short circuit test at room temperature shows a high power loss component (1.1kW) at 19.2A. This is much higher than the power loss in the short circuit test at liquid nitrogen temperature (410W at 30.6A). This is explained by the difference in winding resistances for the two different operating temperatures.

Table 5.8 give a comparison between the test and the model results. The model is simulated with the core operating at 17.6°C, inside winding operating at 45.4°C and the outside winding operating at 29.4°C. The difference in the ESLs is a major factor in the accuracy of the model. This is discussed further in section 5.4.2.

5.4 SUPERCONDUCTING TRANSFORMER

5.4.1 Test Results

Tables 5.9 to 5.16 give the results of the superconductor tests performed at LN2 temperature. The temperature of the windings of the transformer stayed constant throughout

Table 5.8 Comparison between the copper mock up transformer test results and the model, operating at room temperature

	Test results		Model		
Winding	Inside	Outside	Inside	Outside	
Voltage	228	195	230	203.5	V
Current	9.96	9.54	9.94	9.83	A
Real power	2.27	1.86	2.28	2.0007	kW
Apparent power	2.27	1.86	2.29	2.0007	kVA
Power Factor	0.99	0.99	0.9987	1	
Phase	1.6	1.25	2.92	0	°
ESR	22.88	-	23.07	-	Ω
ESL	0.64	-	0.48	-	Ω
Efficiency		81.62		87.75	%
Voltage Regulation		13.34		10.33	%

all the tests, the voltage of the K-type temperature probe was at ~ -6.5mV. There was no significant LN2 boil off in most of the tests. During the 60A load test, there was slightly more boil off compared to the open circuit test.

Table 5.9 SCTX Open circuit test results, operated at liquid nitrogen

Open circuit test		
Primary voltage	226	V
Primary current	0.26	A
Primary power	34	W
Primary apparent power	57	VA
Primary Power factor	0.59	
Secondary voltage	232	V
Voltage ratio	0.97	

Table 5.10 SCTX Short circuit test results, operated at liquid nitrogen

Short circuit test		
Primary voltage	40.2	V
Primary current	35	A
Primary power	0.07	kW
Primary apparent power	1.41	kVA
Primary Power factor	0.05	
Secondary current	33.5	A
Current ratio	1.04	

Table 5.11 SCTX 10A endurance test (2 minutes) results operated at liquid nitrogen

10A endurance test					
Primary voltage	232	V	Secondary voltage	234.6	V
Primary current	10.41	A	Secondary current	10.05	A
Primary power	2.29	kW	Secondary power	2.29	kW
Primary apparent power	2.41	kVA	Secondary apparent power	2.36	kVA
Primary Power factor	0.95		Secondary power factor	0.97	
Efficiency	100%				
Voltage regulation	4.24%				

Table 5.12 SCTX 20A endurance test (2 minutes) results operated at liquid nitrogen

20A endurance test					
Primary voltage	232.1	V	Secondary voltage	222.5	V
Primary current	19.7	A	Secondary current	19.1	A
Primary power	4.2	kW	Secondary power	4.1	kW
Primary apparent power	4.4	kVA	Secondary apparent power	4.2	kVA
Primary Power factor	0.94		Secondary power factor	0.97	
Efficiency	99.31	%			
Voltage regulation	2.87	%			

Table 5.13 SCTX 30A endurance test (2 minutes) results operated at liquid nitrogen

30A endurance test					
Primary voltage	227.1	V	Secondary voltage	220.7	V
Primary current	31.7	A	Secondary current	31.7	A
Primary power	6.6	kW	Secondary power	6.5	kW
Primary apparent power	7.2	kVA	Secondary apparent power	6.8	kVA
Primary Power factor	0.91		Secondary power factor	0.96	
Efficiency	98.67	%			
Voltage regulation	5.35	%			

Table 5.17 shows the resistance of the windings before, during and after submerging the transformer in LN2. The readings taken during submersion were measured from the lead ends. As putting the cables of the micro-ohm meter in LN2 would have damaged them. In hindsight, the cables could be connected before filling and thus would not suffer from thermal shock.

Table 5.11 shows that the meters did not have sufficient resolution to determine

Table 5.14 SCTX 40A endurance test (2 minutes) results operated at liquid nitrogen

40A endurance test					
Primary voltage	229.1	V	Secondary voltage	218.5	V
Primary current	41.1	A	Secondary current	40.1	A
Primary power	8.6	kW	Secondary power	8.4	kW
Primary apparent power	9.4	kVA	Secondary apparent power	8.8	kVA
Primary Power factor	0.91		Secondary power factor	0.96	
Efficiency	98.35	%			
Voltage regulation	7.11	%			

Table 5.15 SCTX 50A endurance test (2 minutes) results operated at liquid nitrogen

50A endurance test					
Primary voltage	231.1	V	Secondary voltage	211.6	V
Primary current	51.7	A	Secondary current	50.5	A
Primary power	10.6	kW	Secondary power	10.4	kW
Primary apparent power	11.9	kVA	Secondary apparent power	10.7	kVA
Primary Power factor	0.88		Secondary power factor	0.97	
Efficiency	97.94	%			
Voltage regulation	10.79	%			

Table 5.16 SCTX 60A endurance test (3 minutes) results operated at liquid nitrogen

60A endurance test					
Primary voltage	230.16	V	Secondary voltage	204.47	V
Primary current	61.98	A	Secondary current	60.54	A
Primary power	12.46	kW	Secondary power	12.04	kW
Primary apparent power	14.26	kVA	Secondary apparent power	12.38	kVA
Primary Power factor	0.87		Secondary power factor	0.97	
Efficiency	96.59	%			
Voltage regulation	13.45	%			

the efficiency accurately. These results were recalculated with higher resolution by reconstructing the voltage and current waveforms via Fourier equations, this is discussed further in section 5.4.2.

Before each load test (table 5.18 to 5.16), the resistances of the windings were checked. The resistances did not change throughout the entire experiment.

Table 5.17 DC resistance of the superconducting windings

	Inside winding	Outside winding	Temperature	
Before submersion	3.046Ω	4.850Ω	20.7°C	at terminals
Full submersion	7.2mΩ	13.7mΩ	-196°C	at lead ends
After submersion	3.03Ω	4.87Ω	17.1°C	at terminals

5.4.2 Discussion

Table 5.18 SCTX 10A endurance test (2 minutes) results operated at liquid nitrogen (Recalculated)

10A endurance test					
Primary voltage	232.1	V	Secondary voltage	234.6	V
Primary current	10.4	A	Secondary current	10.1	A
Primary power	2.3	kW	Secondary power	2.3	kW
Primary apparent power	2.4	kVA	Secondary apparent power	2.4	kVA
Primary Power factor	0.94		Secondary power factor	0.96	
Efficiency	99.39	%			
Voltage regulation	1.54	%			

Table 5.11 gives the 10A endurance run test performed on the SCTX operating at liquid nitrogen. From the primary and secondary power readings, it was calculated that the efficiency was 100%. However, the meters give rounded values, not providing sufficient resolution to discriminate the differences between the real powers on either side of the transformer. The Fluke®41 meters contain extra information such as the magnitudes and phases of all the harmonics. This can be used to reconstruct the voltage and current waveform via Fourier equations. Hence, the RMS voltage, current, power factor, real power and apparent power can be recalculated with greater resolution. Table 5.18 shows the recalculated values of the 10A endurance run.

Table 5.9 shows the open circuit test results of the SCTX operating at LN2 temperature. The results show a higher real power loss compared to the open circuit test of the copper mockup transformer at LN2 temperature. This might be due to reassembling the core slightly differently during the SCTX building phase. Regardless, the power dissipated from the core would not be a large heat contributor for LN2 boil off. The secondary voltage shows that the transformer is a slight step up. This is due to adding more turns on the outside winding (secondary) to compensate for the high voltage regulation seen in the CTX (table 5.3).

The short circuit test (table 5.10) shows that there is 70W of losses. In chapter 3, the hysteresis constant, P_{ref}, needs to be obtained via a pick-up coil method [4]. In [4],

the magnetisation loss was measured on a single tape and P_{ref} was fitted to those experimental results. The reference field was 0.1T, 50Hz at 77K.

However, the lack of equipment available means that the model needs to be matched using other methods. In a short circuit test, the winding losses are dominant. This means that P_{ref} can be matched using the short circuit test results. Table 5.19 shows the short circuit simulation results of the transformer.

Table 5.19 SCTX Short circuit simulation results, operated at liquid nitrogen

Short circuit test		
Primary voltage	40.2	V
Primary current	33.23	A
Primary power	0.067	kW
Primary apparent power	1.34	kVA
Primary Power factor	0.05	
Secondary current	32.32	A
Current ratio	0.97	
p_{ref}	3	$\mathrm{WA^{-1}m^{-1}}$

Table 5.17 shows the resistance test before, during and after submerging the transformer in liquid nitrogen. The results indicate that there was no damage to the windings after the testing. The results do not show conclusively that the windings were superconducting. More tests under liquid nitrogen will have to be undertaken to confirm superconduction.

Tables 5.18 to 5.16 show that the efficiency decreased as the load is increased. This shows that the windings have increased losses as the load current increases (assuming the core losses are constant). The maximum efficiency of the transformer was 99.4% at a 10A load current. The worst efficiency was 96.6% at a 60A load. The SCTX shows a significant improvement over the CTX in terms efficiency and voltage regulation, despite having the same dimensions. The SCTX also endured the 60A load test for 3 minutes, which was longer than what the PCTX endured(chapter 2). This suggests that the cooling channels have improved the performance significantly and have reduced the chances of failure. Also the SCTX would have less leakage flux compared to the PCTX, due to the full core design. This would further decrease the amount of winding losses as well as reduce the chances of the superconductor quenching.

Tables 5.20 to 5.25 give the comparisons between the test and model results of the superconducting transformer at different loads. The comparisons show that there is a significant difference between the test result ESL and the model ESL. This was also observed in the copper mock up tests. It is observed in tables 5.20 to 5.25 that the ESL varies with the load current. This points to evidence that the inductance changes with current indirectly. In Bell [27], it was observed that the flux patterns of a full core

transformer varies depending on how it is connected. For example, an open circuit test on a transformer would produce a flux pattern that is completely different to that of the transformer under short circuit conditions. This would mean at different load currents, the flux patterns would be different. In effect, the flux density will not be uniform at low loads. The non-uniform flux patterns would then vary the effective cross-sectional area in which the flux flows through, which would in turn affect the inductance of the transformer. This would mean that the reactance model (given in chapter 3) would only be most accurate near full load current. This is observed in table 5.25, where the test result ESL is quite close to the model ESL.

Table 5.20 Comparison between results and model, 10A loaded current

	Test results		Model		
Winding	Inside	Outside	Inside	Outside	
Voltage	232.14	234.6	232.14	238.09	V
Current	10.4	10.1	10.41	9.96	A
Real power	2.3	2.3	2.41	2.37	kW
Apparent power	2.4	2.4	2.42	2.37	kVA
Power factor	0.94	0.96	0.99	1	
Phase	19.02	15.71	3.83	0	°
ESR	21.08	-	22.25	-	Ω
ESL	7.26	-	1.49	-	Ω
Efficiency		99.4		98.36	%
Voltage regulation		1.5		0.09	%

Table 5.21 Comparison between results and model, 20A loaded current

	Test results		Model		
Winding	Inside	Outside	Inside	Outside	
Voltage	223.13	222.5	223.13	227.68	V
Current	19.8	19.1	19.75	19.05	A
Real power	4.2	4.1	4.38	4.34	kW
Apparent power	4.4	4.2	4.41	4.34	kVA
Power factor	0.95	0.98	0.99	1	
Phase	18.87	12.63	6.49	0	°
ESR	10.69	-	11.23	-	Ω
ESL	3.65	-	1.28	-	Ω
Efficiency		99.32		99.07	%
Voltage regulation		2.88		0.59	%

To improve the reactance model, a new factor can be introduced to correct the reactances. This is obtained by using the test ESL and dividing it by the model ESL.

Table 5.22 Comparison between results and model, 30A loaded current

	Test results		Model		
Winding	Inside	Outside	Inside	Outside	
Voltage	227.12	220.7	227.12	229.37	V
Current	31.7	31.7	31.72	30.69	A
Real power	6.6	6.5	7.09	7.04	kW
Apparent power	7.2	6.8	7.21	7.04	kVA
Power factor	0.92	0.96	0.98	1	
Phase	23.37	15.85	9.91	0	°
ESR	6.57	-	7.05	-	Ω
ESL	2.83	-	1.23	-	Ω
Efficiency		98.67		99.21	%
Voltage regulation		5.35		1.62	%

Table 5.23 Comparison between results and model, 40A loaded current

	Test results		Model		
Winding	Inside	Outside	Inside	Outside	
Voltage	229.14	218.5	229.14	228.78	V
Current	41.2	40.1	41.16	39.87	A
Real power	8.6	8.4	9.2	9.12	kW
Apparent power	9.4	8.8	9.43	9.12	kVA
Power factor	0.91	0.96	0.98	1	
Phase	24.5	15.4	12.67	0	°
ESR	5.07	-	5.43	-	Ω
ESL	2.31	-	1.22	-	Ω
Efficiency		98.35		99.15	%
Voltage regulation		7.12		2.74	%

This factor is called the L-factor and is plotted against the inside winding current shown in figure 5.4. The equation of the fitted curve in figure 5.4 is $24.62\times\mathrm{I}^{-0.7}$, where I is the current. This factor is then inserted into the winding reactance calculations. This is shown in equation 5.2.

$$X_{12} = 24.62 \times I^{-0.7} \times \frac{\omega \mu_0 N_1^2}{l_c} \left[\frac{l_p d_1 + l_s d_2}{3} + l_{ps} \Delta d \right] \tag{5.2}$$

However, equation 5.2 would not be entirely correct as the L-factor is calculated from an equivalent circuit which means that the core reactance was taken into account. However, this would produce a more accurate result than without having the L-factor correction. Tables 5.26 to 5.31 shows the comparison between the test results and the

Table 5.24 Comparison between results and model, 50A loaded current

	Test results		Model		
Winding	Inside	Outside	Inside	Outside	
Voltage	231.12	211.6	231.12	227.09	V
Current	51.7	50.5	51.66	50.09	A
Real power	10.6	10.4	11.49	11.38	kW
Apparent power	11.94	10.7	11.94	11.38	kVA
Power factor	0.89	0.97	0.96	1	
Phase	27.5	13.9	15.77	0	°
ESR	3.97	-	4.31	-	Ω
ESL	2.06	-	1.22	-	Ω
Efficiency		97.95		99	%
Voltage regulation		10.8		4.28	%

Table 5.25 Comparison between results and model, 60A loaded current

	Test results		Model		
Winding	Inside	Outside	Inside	Outside	
Voltage	230.16	204.47	230.16	221.52	V
Current	62.0	60.5	61.98	60.13	A
Real power	12.5	12.0	13.48	13.32	kW
Apparent power	14.3	12.4	14.27	13.32	kVA
Power factor	0.87	0.97	0.95	1	
Phase	29.14	13.51	19.06	0	°
ESR	3.24	-	3.51	-	Ω
ESL	1.81	-	1.21	-	Ω
Efficiency		96.5971		98.7918	%
Voltage regulation		13.4571		6.2444	%

modified model with the L-factor correction.

Table 5.32 shows the summary of the before and after effects of adding the L-factor correction.

The modified model has produced better results compared to those before using the L-factor correction. Further testing is required to accurately determine the correction factors to X_1, X_2 and X_M individually.

Table 5.33 shows the percentage differences of ESR and ESL between the test results and the old/new model. The ESR differences of the old model and the new model are not a good indication of how good the superconductor model is. This is due to the load dominating the equivalent circuit. There are also other factors such as the empirical equations used to calculate the losses in the tape. A more accurate

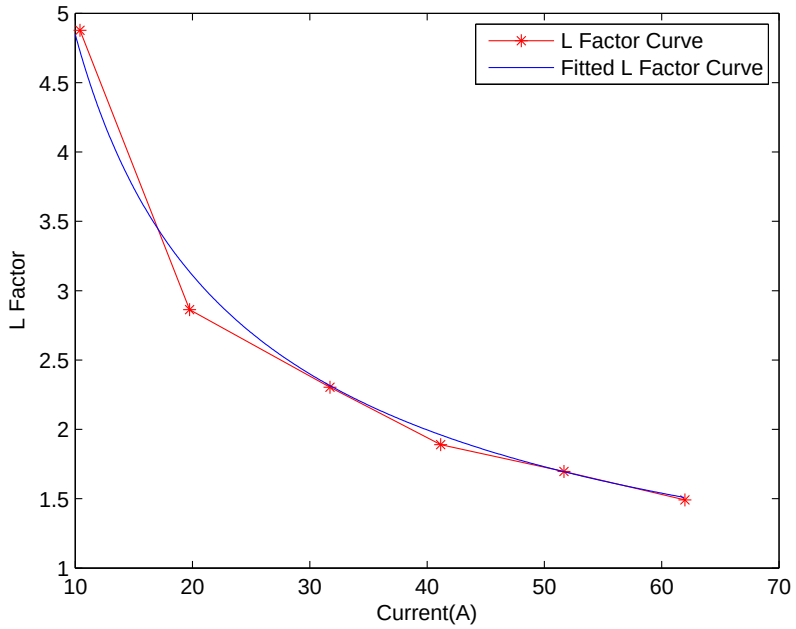

Figure 5.4 L Factor of the superconducting transformer.

Table 5.26 Comparison between results and modified model, 10A loaded current

	Test results		Model		
Winding	Inside	Outside	Inside	Outside	
Voltage	232.14	234.64	232.14	230.18	V
Current	10.4	10.1	10.40	9.95	A
Real power	2.3	2.3	2.32	2.29	kW
Apparent power	2.4	2.4	2.41	2.29	kVA
Power factor	0.94	0.96	0.96	1	
Phase	19.02	15.71	15.51	0	°
ESR	21.09	-	21.50	-	Ω
ESL	7.26	-	5.97	-	Ω
Efficiency		99.39		98.38	%
Voltage regulation		1.54		3.41	%

solution is to use the pick-coil method to accurately measure the coefficients of the superconductor losses and implementing these into the model [20].

The L-factor (equation 5.2) can only be used for this transformer. This is because the L-factor does not take into account what other variables might affect the reactance, such as the aspect ratio [16]. Similarly, this L-factor cannot be used for open circuit calculations or short circuit calculations as the flux patterns would be different compared to loaded conditions [27]. A new L-factor would be needed for the copper mockup transformer as well.

Table 5.27 Comparison between results and modified model, 20A loaded current

	Test results		Model		
Winding	Inside	Outside	Inside	Outside	
Voltage	223.12	222.5	223.12	216.41	V
Current	19.7	19.1	19.77	19.07	A
Real power	4.2	4.1	4.16	4.13	kW
Apparent power	4.4	4.2	4.41	4.13	kVA
Power factor	0.95	0.98	0.94	1	
Phase	18.87	12.63	19.26	0	°
ESR	10.69	-	10.65	-	Ω
ESL	3.65	-	3.72	-	Ω
Efficiency		99.32		99.09	%
Voltage regulation		2.88		5.52	%

Table 5.28 Comparison between results and modified model, 30A loaded current

	Test results		Model		
Winding	Inside	Outside	Inside	Outside	
Voltage	227.12	220.7	227.12	216.22	V
Current	31.7	31.7	31.73	30.69	A
Real power	6.6	6.5	6.69	6.64	kW
Apparent power	7.2	6.8	7.21	6.64	kVA
Power factor	0.92	0.96	0.93	1	
Phase	23.37	15.85	21.8	0	°
ESR	6.57	-	6.65	-	Ω
ESL	2.84	-	2.66	-	Ω
Efficiency		98.67		99.2	%
Voltage regulation		5.35		7.26	%

The SCTX was also tested under open circuit conditions at room temperature. The resulting voltage and magnetising current waveforms are shown in figure 5.5. The magnetising current has a dominant 3rd harmonic content and causes the large spike. The magnitudes of the current peaks do not scale linearly with the increase in voltage, i.e. a 50V (21%) increase in voltage resulted in a 0.5A (100%) increase in the current peak magnitudes. It is also noted that the supply voltage is not a pure sinusoid which plays a big factor in introducing harmonics which leads to larger 3rd harmonic peaks. The model described in chapter 3 has not taken these non-linearities into account.

The advantage of having the SCTX is the reduction in cable size and hence reduction in total weight and size of the transformer. A typical copper winding 15kVA transformer weighs approximately 70kgs, not including the coolant. The measured weight of the SCTX was 37.3kgs, the model predicted a metal weight of 25.4kgs which

Table 5.29 Comparison between results and modified model, 40A loaded current

	Test results		Model		
Winding	Inside	Outside	Inside	Outside	
Voltage	229.14	218.5	229.14	215.18	V
Current	41.2	40.1	41.15	39.87	A
Real power	8.6	8.4	8.64	8.58	kW
Apparent power	9.4	8.8	9.43	8.58	kVA
Power factor	0.91	0.96	0.92	1	
Phase	24.49	15.42	23.66	0	°
ESR	5.07	-	5.1	-	Ω
ESL	2.31	-	2.24	-	Ω
Efficiency		98.35		99.32	%
Voltage regulation		7.12		8.52	%

Table 5.30 Comparison between results and modified model, 50A loaded current

	Test results		Model		
Winding	Inside	Outside	Inside	Outside	
Voltage	231.11	211.6	231.11	213.97	V
Current	51.7	50.5	51.65	50.08	A
Real power	10.6	10.4	10.83	10.72	kW
Apparent power	11.9	10.7	11.94	10.72	kVA
Power factor	0.88	0.97	0.91	1	
Phase	27.45	13.90	24.9	0	°
ESR	3.97	-	4.06	-	Ω
ESL	2.06	-	1.88	-	Ω
Efficiency		97.95		98.97	%
Voltage regulation		10.79		9.81	%

does not include the weight of the insulation, spacers, fasteners, copper terminations and the termination plate.

The efficiency of the SCTX is comparable to similarly rated copper transformer, however if a cryogenic cooler was installed, the efficiency of the SCTX would drop significantly. The alternative is to design an efficient dewar, where the LN2 losses from heat from the ambient air is minimal. Hence, it would only require a LN2 top up when the LN2 level is low. The demand of LN2 would increase as the the superconductor technology matures. This would lead to a decrease in price and the operational cost of LN2 would be insignificant. An economic comparison between the cryogenic cooler option and the efficient dewar option needs to be made in order to determine which is the best option.

Table 5.31 Comparison between results and modified model, 60A loaded current

	Test results		Model		
Winding	Inside	Outside	Inside	Outside	
Voltage	230.16	204.48	230.16	209.66	V
Current	62.0	60.5	61.92	60.074	A
Real power	12.5	12.0	12.75	12.59	kW
Apparent power	14.3	12.4	14.25	12.59	kVA
Power factor	0.87	0.97	0.89	1	
Phase	29.14	13.51	26.49	0	°
ESR	3.24	-	3.33	-	Ω
ESL	1.81	-	1.66	-	Ω
Efficiency		96.6		98.75	%
Voltage regulation		13.46		11.26	%

Table 5.32 Summary of the changes to ESR and ESL after modifying the model

		Test Results	Old model	New model	
10A load	ESR	21.09	22.25	21.5	Ω
	ESL	7.27	1.49	5.97	Ω
20A load	ESR	10.69	11.23	10.65	Ω
	ESL	3.65	1.28	3.72	Ω
30A load	ESR	6.57	7.05	6.65	Ω
	ESL	2.84	1.23	2.66	Ω
40A load	ESR	5.07	5.43	5.1	Ω
	ESL	2.31	1.22	2.23	Ω
50A load	ESR	3.97	4.31	4.06	Ω
	ESL	2.06	1.22	1.88	Ω
60A load	ESR	3.24	3.51	3.33	Ω
	ESL	1.81	1.21	1.66	Ω

5.5 FUTURE WORK

5.5.1 Electrical Testing

There is potential for more improvement of the superconductor loss model (R_1 and R_2 in the Steimetz equivalent circuit) as well as the reactance model (X_1 and X_2 in the Steimetz equivalent circuit) of the SCTX. For the reactance model, new correction factors are needed for different short circuit and loaded circuit currents. Further study is also required to determine how the correction factors would affect other transformers including the CTX. This would lead to determining other variables that influence the leakage reactances. Also, the new reactance model can be compared to the finite

Table 5.33 Percentage difference of ESR and ESL model compared to the test results

		Old model	New model	
10A load	ESR	5.54	1.97	%
	ESL	79.5	17.93	%
20A load	ESR	5.01	0.36	%
	ESL	65.07	1.89	%
30A load	ESR	7.3	1.15	%
	ESL	56.6	6.38	%
40A load	ESR	7.21	0.66	%
	ESL	47.04	3.2	%
50A load	ESR	8.45	2.25	%
	ESL	41.04	8.62	%
60A load	ESR	8.21	2.57	%
	ESL	32.93	8.3	%

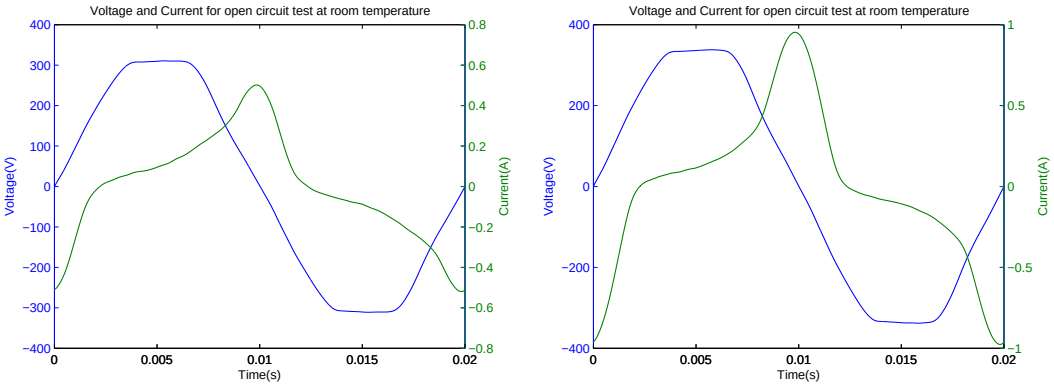

(a) 230V Open circuit

(b) 250V Open circuit

Figure 5.5 Voltage and current waveforms of the different open circuit tests at room temperature.

element analysis FEA model [7].

The superconductor loss model is based on theoretical flux density equations. This can be improved if experimental data can be obtained on the leakage flux densities. This would involve using hall effect sensors which can be installed at the winding layer gaps. This data can be used to compare with that from the theoretical flux model and further improve the superconductor loss model.

Based on observation of the magnetising current (figure 5.5), the core model can be improved. Currently the model assumes that a pure sinusoidal voltage is applied and that the core magnetisation curve is linear. The core model needs to include a changing impedance due to the different frequencies applied by the non-ideal voltage waveform of the supply. This could be implemented for the leakage reactances and could account for some of the differences seen in the ESLs of the test results.

A sensitivity analysis can be performed on the coefficients of the superconductor model. The purpose would be to see how much the simulation results vary with changes in the coefficients.

Both the transformers need to be tested for long term operation. This would involve testing under different load conditions. The experiments have indicated that the SCTX may withstand higher loads as well. However, the duration of these tests are limited by the supply of and rate of boil-off of LN2 in the existing dewar.

The core of the transformer was built in a way that it could operate in partial core mode. Both the transformers could be tested in this configuration to provide additional research data.

A protection circuit should be implemented if the SCTX is operating for a long duration. The protection circuit would need to detect whether the tape has quenched at any time. The parameters of detection would include a sudden change in the impedance of the transformer, assuming the load has not changed. This would involve constantly measuring the impedance of the primary side and secondary side (if there is a varying load impedance). The equivalent transformer impedance could then be calculated. A sudden change in this impedance would suggest the wire has quenched. Other parameters, such as the temperature of the windings, pressure build-up inside the dewar and excessive LN2 boil-off should also be included in the protection scheme. A LN2 level alarm should also be installed for long term operation, which would alert for the need for LN2 filling.

5.5.2 Mechanical Work

The dewar used for experimentation is not good enough for long term operation. A more efficient design is required for the SCTX. A proposed design, described briefly in chapter 4, is a double skinned dewar which separates the cooling in the windings from the core. The proposed design would no longer work for the current SCTX as a new core would have to be built. However, a new, simpler and cheaper design could be implemented to submerge the entire SCTX in the dewar. This could coincide with designing and building a new transformer mounting bracket, that allows the whole transformer to be easily brought out of the dewar via crane or hand crank. The problem encountered in the current design was that the SCTX was being placed inside the dewar by hand. During LN2 submersion, the SCTX was not able to be brought out of the dewar. This is so that if the connections to the terminals become loose, the transformer could be easily brought out to make the necessary repairs.

The laminations of the core started to rust during the defrosting stage after each experiment. Although it would take a long time for the core to deteriorate, it is undesirable to have the core rusting. A resin coating could be applied to the laminations of the limbs and yokes. However, the yokes and limbs cannot be resined together as

that would defeat the purpose of this project, which is to have a core and two different windings that can be easily switched.

The layer insulation is made out of fibreglass rectangular bars. Due to the sharp corners of the rectangular bars, additional work was required to sand the corners to ensure that they did not kink the superconductor. This was a lengthy process and a better solution is to have fibreglass rods replace the rectangular bars. However, there were no fibreglass manufacturers that would make the rods cheaply, hence the decision was made to use the rectangular bars. For the future design of new superconducting windings it is recommended that fibreglass rods are used. Custom made tubes with cooling channels is also a better design for the layer insulation, however the cost of manufacturing these could be quite high.

5.6 ESTIMATED COST AND BUILDING TIME

This section details the estimated cost of the two windings and the transformer core. The estimated building time of each component is also given.

5.7 CONCLUSION

The results of the testing done on the CTX and SCTX were presented. The open circuit test on the CTX immersed in LN2 showed 19W of power loss in the core. The CTX short circuit test in LN2 showed 410W of losses at 30.6A. The CTX loaded test in LN2 resulted in an 88.2% efficiency and a 16.16% voltage regulation at an 11.2kVA load. The CTX was then tested at room temperature. The open circuit test showed a lower power loss (16W) compared to that of the open circuit test at LN2 temperature. The room temperature short circuit test resulted in 1.1kW of power loss at 19.2A. The 10A load endurance run at room temperature resulted in an 81.9% efficiency and a 12.73% voltage regulation with a 2.27kVA load. The major difference between the test results and the model was the ESL, which was 51.97%.

Next, the SCTX was tested at LN2 temperatures. When the SCTX was fully submerged in LN2, the measured DC resistance was 7.2mΩ on the inside winding and 13.7mΩ on the outside winding. However, the resistance measure is dominated by the lead and terminal resistances. The open circuit test of the SCTX in LN2 showed 34W of power loss with an inside winding excitation of 226V. The short circuit test in LN2 showed 70W of losses in the windings at 35A. The load tests showed that the maximum efficiency achieved by the SCTX was 99.39% at a 2.28kVA load and a minimum efficiency of 96.59% at a 14.26kVA load. The simulated results showed that the reactances calculated were lower than those determined from the test results. This prompted a correction factor to be included in the model. The resulting correction has brought the model simulated results closer to the test results. However, more testing is

Table 5.34 Estimated cost and building time of the CTX and SCTX

		Estimated cost	Estimated time
Core			
-	Cutting laminations	-	2 months
-	Material cost	$225.16	
Copper Windings			
-	Insulation process	-	1 month
-	Fibreglass spacers (cutting)	-	1 week
-	Winding process	-	2 weeks
-	Copper material cost	$100.00	
-	Insulation tape	$57.80	
-	Fibreglass material cost	$40.00	
-	Winding former	$5.00	
Superconducting windings			
-	Insulation process	-	2 weeks
-	Fibreglass spacers (cutting)	-	1 week
-	Winding process	-	1 week
-	Soldering	$50.00	1 week
-	Superconductor cost	$17,373.60	
-	Fibreglass material cost	$40.00	
-	Winding former	$5.00	
Other			
-	Terminations and plate	$15.00	
-	Steel Fasteners	$10.00	
-	Nuts and bolts	$5.00	
-	K-type temperature probes	$50.00	
-	Assembly time	-	1 month
-	Liquid nitrogen	$360	
Total		$18,336.56	5 months

required to refine the correction factor and to introduce new factors for different circuit configurations.

There is potential for additional testing and mechanical improvement of the SCTX. A protection circuit and a more efficient dewar needs to be built before the SCTX can be put into long term operation. The core of the transformer got rusty after each defrosting period, this means it should be resined to prevent more deterioration. Optionally, a transformer bracket can be built for ease of moving and taking the transformer out of the dewar. Additional testing includes operating the transformers in partial core mode, and long term tests with load.

Chapter 6

CONCLUSION

This thesis began with the testing of a partial core superconducting transformer. The transformer was subjected to open circuit, short circuit, full load and a full load endurance test in LN2. This resulted in a failure during the full load endurance test. The investigation into the failure started off with calculating the field strengths of the leakage flux. The leakage flux strength was found to be insufficient to quench the superconductor. Further testing revealed that the transformer inside winding was disconnected and had a shorted turn. The windings were taken apart and it was revealed that most of the damage had occurred in the inside winding. The burn profile indicated that the superconductor quenched due to a lack of cooling. The resulting quench caused the winding to fuse and burn out.

Chapter 3 described the techniques used for designing the full core copper and full core superconducting transformers using the Steimetz equivalent circuit and reverse design techniques. The superconductor loss model uses AC loss theory to describe the winding resistances in the Steinmetz equivalent circuit. The AC loss theory requires the leakage field strengths to calculate the losses. This prompted the use of a leakage flux model, which describes the flux densities in the winding layer gaps of the transformer.

In chapter 4, the designs of the two transformers were given. The properties and design data of the two windings and core were described. A CAD for the CTX was graphically presented. The step by step processes in the construction phase of the transformers were also given. The dimensions and the process of cutting of the core pieces was described. The process of insulating the copper and superconductor tapes was also shown. Additional features were added to the transformers, such as the steel fasteners, terminations and a terminal plate.

Finally, chapter 5 gave the results of testing both the CTX and the SCTX. The CTX was tested under open circuit, short circuit, and full load tests in both LN2 and at room temperature. The SCTX was tested under open circuit, short circuit, and various load tests in LN2 and at room temperature. The CTX open circuit test (LN2) showed 19W of power loss, which is dominated by the core loss. The CTX short circuit test in LN2 resulted in 410W of losses at 30.6A, which are dominated by the winding

losses. The CTX load test in LN2 resulted in an 88.2% efficiency and a 16.2% voltage regulation at an 11.2kVA load. The CTX room temperature open circuit test showed a power loss of 16W. The CTX room temperature short circuit test showed a power loss of 1.1kW at 19.2A. The CTX 10A load endurance run at room temperature resulted in a 81.9% efficiency and a 12.7% voltage regulation with a 2.27kVA load at unity power factor. The anomaly observed between the CTX test and model results was the ESL, which was different by 51.9%. The SCTX open circuit test in LN2 resulted in 34W of losses, which is larger than the CTX open circuit test even though the same core was used. This change was attributed to assembling the core slightly differently. The SCTX short circuit test in LN2 showed 70W of losses, dominated by the windings, at 35A. The various SCTX load tests in LN2 showed a decreasing efficiency as the load was increased. The maximum efficiency of 99.4% was achieved at a 2.28kVA load and the lowest efficiency of 96.6% was achieved at a 14.26kVA load. The superconducting winding transformer was shown to exceed the copper winding transformer in terms of efficiency and voltage regulation. Next, the test results were compared with the model results. The same anomaly, observed in the CTX testing, was observed in the comparison. This prompted a correction factor to be included into the model. The introduction of this correction factor vastly improved the model accuracy. However, additional testing is required to introduce more correction factors for different circuit configurations and different transformers. There is further work that needs to be done to improve the mathematical models used in chapter 3. This would include the pick up coil method which would improve the empirically dependant superconductor AC loss formulas. Mechanical improvements and a protection circuit need to be implemented before testing the SCTX for long term operation.

REFERENCES

[1] R. Pengo, K. Barth, N. Delruelle, M. Pezzetti, O. Pirotte, G. Passardi, A. Dudarev, and H. ten Kate, "Cryogenic characteristics of the atlas barrel toroid superconducting magnet," *IEEE Trans. Appl. Supercond.*

[2] J. Bardeen, L. N. Cooper, and J. R. Schrieffer, "Theory of superconductivity," *Physical Review*, vol. 108, no. 5, p. 1175, 1957.

[3] V. Ginzburg, "On the theory of superconductivity," *Il Nuovo Cimento (1955-1965)*, vol. 2, no. 6, pp. 1234–1250, 1955.

[4] M. P. Oomen, R. Nanke, and M. Leghissa, "Modelling and measurement of ac loss in bscco/ag-tape windings," *Superconductor Science and Technology*, no. 3, p. 339, 2003.

[5] P. S. Bodger, W. G. Enright, and K. W. V. Ho, "A low-voltage, mains frequency partial core, high temperature, superconducting transformer," *Australasian Universities Power Engineering Conference - AUPEC 2005, Hobart, Australia*, 2005.

[6] P. S. Bodger, D. Harper, M. Gazzard, M. O'Neill, and W. G. Enright, "Towards a usable mains frequency partial core transformer," *Australasian Universities Power Engineering Conference, AUPEC 2002. Australasia.*

[7] S. C. Bell and P. S. Bodger, "Power transformer design using magnetic circuit theory and finite element analysis; a comparison of techniques," *Australasian Universities Power Engineering Conference, AUPEC 2007. Australasia*, pp. 1–6, 2007.

[8] A. Heinrich, "Quenching of superconductivity and propagation of the resulting normal phase in ybco films," *Superconductor Science and Technology*, no. 10, p. 1354, 2005.

[9] Y. Zhou, Y. Tang, J. Li, B. Wei, and J. Shi, "Quench and recovery behaviors of bi-2223/ag hts tapes under pulsed over-currents with different durations," *Physica C: Superconductivity*, vol. 433, no. 1-2, pp. 37–42, 2005.

[10] L. N. Cooper, "Bound electron pairs in a degenerate fermi gas," *Physical Review*, vol. 104, no. 4, p. 1189, 1956.

[11] Y. Kamihara, T. Watanabe, M. Hirano, and H. Hosono, "Iron-based layered superconductor la-o-fe-p with tc = 26 k," *American Chemical Society*, vol. 130, no. 11, pp. 3296–3297, 2008.

[12] H. Takahashi, K. Igawa, K. Arii, Y. Kamihara, M. Hirano, and H. Hosono, "Superconductivity at 43-k in an iron-based layered compound la-o-f-fe-as," *Nature*, vol. 453, no. 7193, pp. 376–378, 2008.

[13] M. C. Liew and P. S. Bodger, "Partial-core transformer design using reverse modelling techniques," *Electric Power Applications, IEE Proceedings*, vol. 148, no. 6, pp. 513–519, 2001.

[14] M. C. Liew, M. B. O'Neill, and P. S. Bodger, "Operating partial core transformers under liquid nitrogen conditions," *Electric Power Applications, IEE Proceedings*, vol. 148, no. 4, pp. 293–298, 2001.

[15] G. R. Slemon, *Magnetoelectric Devices: transducers, transformers and machines.* John Wiley and Sons, Inc., 1966.

[16] M. C. Liew and P. S. Bodger, "Applying a reverse design modelling technique to partial core transformers," no. 20, pp. 310–315, 2001.

[17] J. Carr, W., "Ac loss from the combined action of transport current and applied field," *IEEE Transactions on Magnetics*, vol. 15, pp. 240–243, Jan 1979.

[18] S. Kawabata, H. Tsuzura, Y. Fukuda, K. Funaki, and K. Osamura, "Standardization of the pickup coil method for ac loss measurement of three-component superconducting wires," *Physica C: Superconductivity*, vol. 392-396, no. Part 2, pp. 1129 – 1133, 2003.

[19] J. J. Rabbers, B. ten Haken, O. A. Shevchenko, and H. H. J. ten Kate, "An engineering formula to describe the ac loss of bscco/ag tape," *Applied Superconductivity, IEEE Transactions on*, vol. 11, no. 1, pp. 2623–2626, 2001.

[20] M. Oomen, "Ac loss in superconducting tapes and cables," *PHD Thesis, University of Twente, Netherlands*, 2000.

[21] K. Namjoshi and P. Biringer, "Low-frequency eddy-current loss estimation in long conductors by using the moment of inertia of cross sections," *Magnetics, IEEE Transactions on*, vol. 24, pp. 2181–2185, Sep 1988.

[22] M. J. Heathcote, *J and P Transformer Book.* Newnes, Elsevier Ltd., 2007.

[23] J. Gerhold, "Cryogenic liquids - a prospective insulation basis for future power equipment," *Dielectrics and Electrical Insulation, IEEE Transactions on*, vol. 9, pp. 68–75, Feb 2002.

[24] C. Sumereder, J. Gerhold, M. Muhr, and R. Woschitz, "Dielectric measurements on hts insulation systems for electric power equipment," *Physica C: Superconductivity and its Applications*, vol. 386, pp. 411–414, 2003.

[25] A. Ilyushechkin, T. Yamashita, P. Talbot, B. Williams, and I. Mackinnon, "Bi-2212/ag laminated tapes: bending and joining effects," *Physica C: Superconductivity and its Applications*, vol. 341-348, pp. IV/–, 2000.

[26] P. S. Bodger, D. Harper, M. Gazzar, M. O'Neill, and W. G. Enright, "The performance of silicon and amorphous steel core, distribution transformers at ambient and cryogenic temperatures," *Australasian Universities Power Engineering Conference - AUPEC 2002, Melbourne, Australia*, 2002.

[27] S. C. Bell, "High-voltage partial-core resonant transformers," *PHD Thesis, University of Canterbury*, 2008.